nature

https://doi.org/10.1038/s41586-021-04342-0

Accelerated Article Preview

Enhanced fitness of SARS-CoV-2 variant of concern Alpha but not Beta

Received: 28 June 2021

Accepted: 13 December 2021

Accelerated Article Preview Published online 22 December 2021

Cite this article as: Ulrich, L. et al. Enhanced fitness of SARS-CoV-2 variant of concern Alpha but not Beta. *Nature* https://doi.org/10.1038/s41586-021-04342-0 (2021).

Lorenz Ulrich, Nico Joel Halwe, Adriano Taddeo, Nadine Ebert, Jacob Schön, Christelle Devisme, Bettina Salome Trüeb, Bernd Hoffmann, Manon Wider, Xiaoyu Fan, Meriem Bekliz, Manel Essaidi-Laziosi, Marie Luisa Schmidt, Daniela Niemeyer, Victor Max Corman, Anna Kraft, Aurélie Godel, Laura Laloli, Jenna N. Kelly, Brenda M. Calderon, Angele Breithaupt, Claudia Wylezich, Inês Berenguer Veiga, Mitra Gultom, Sarah Osman, Bin Zhou, Kenneth Adea, Benjamin Meyer, Christiane Eberhardt, Lisa Thomann, Monika Gsell, Fabien Labroussaa, Jörg Jores, Artur Summerfield, Christian Drosten, Isabella Anne Eckerle, David E. Wentworth, Ronald Dijkman, Donata Hoffmann, Volker Thiel, Martin Beer & Charaf Benarafa

Article

Enhanced fitness of SARS-CoV-2 variant of concern Alpha but not Beta

https://doi.org/10.1038/s41586-021-04342-0

Received: 28 June 2021

Accepted: 13 December 2021

Published online: 22 December 2021

Lorenz Ulrich[1,17], Nico Joel Halwe[1,17], Adriano Taddeo[2,3,17], Nadine Ebert[2,3,17], Jacob Schön[1], Christelle Devisme[2,3], Bettina Salome Trüeb[2,3,4], Bernd Hoffmann[1], Manon Wider[5], Xiaoyu Fan[6], Meriem Bekliz[7], Manel Essaidi-Laziosi[7], Marie Luisa Schmidt[8], Daniela Niemeyer[8,9], Victor Max Corman[8,9], Anna Kraft[1], Aurélie Godel[2,3], Laura Laloli[5,10], Jenna N. Kelly[2,3], Brenda M. Calderon[6], Angele Breithaupt[11], Claudia Wylezich[1], Inês Berenguer Veiga[2,3], Mitra Gultom[5,10], Sarah Osman[6], Bin Zhou[6], Kenneth Adea[7], Benjamin Meyer[12], Christiane Eberhardt[12,13,14], Lisa Thomann[2,3], Monika Gsell[5], Fabien Labroussaa[4], Jörg Jores[4], Artur Summerfield[2,3], Christian Drosten[8,9], Isabella Anne Eckerle[7,15,16], David E. Wentworth[6], Ronald Dijkman[5,18], Donata Hoffmann[1,18], Volker Thiel[2,3,18]✉, Martin Beer[1,18]✉ & Charaf Benarafa[2,3,18]✉

Emerging variants of concern (VOC) drive the SARS-CoV-2 pandemic[1,2]. Experimental assessment of replication and transmission of major VOC compared to progenitors are needed to understand successful emerging mechanisms of VOC[3]. Here, we show that Alpha and Beta spike (S) proteins have a greater affinity to human angiotensin converting enzyme 2 (hACE2) receptor over the progenitor variant (wt-S^{614G}) in vitro. Yet Alpha and wt-S^{614G} had similar replication kinetics in human nasal airway epithelial cultures, whereas Beta was outcompeted by both. In vivo, competition experiments showed a clear fitness advantage of Alpha over the progenitor variant (wt-S^{614G}) in ferrets and two mouse models, where the substitutions in S were major drivers for fitness advantage. In hamsters, supporting high replication levels, Alpha and wt-S^{614G} had comparable fitness. In contrast, Beta was outcompeted by Alpha and wt-S^{614G} in hamsters and hACE2-expressing mice. Our study highlights the importance of using multiple models for complete fitness characterization of VOC and demonstrates adaptation of Alpha towards increased upper respiratory tract replication and enhanced transmission in vivo in restrictive models, whereas Beta fails to overcome contemporary strains in naïve animals.

Uncontrolled transmission of severe acute respiratory syndrome-coronavirus 2 (SARS-CoV-2) in the human population has contributed to the persistence of the coronavirus disease 2019 (COVID-19) pandemic. The emergence of new variants in largely immunologically naïve populations suggests that adaptive mutations within the viral genome continue to improve the fitness of this zoonotic virus towards its host. In March 2020, the single amino acid change in the spike (S) protein at position 614 (S^{D614G}) was identified in only a small fraction of sequenced samples but, within a few weeks, became the most predominant variant worldwide[4]. The fitness advantage conferred by this single amino acid change was supported by a major increase in infectivity, viral loads, and transmissibility *in vitro* and in animal models[3,5,6].

In the second half of 2020, new SARS-CoV-2 variants of concern (VOC) with a combination of several mutations emerged including the Alpha VOC (also known as B.1.1.7), first described in southeast England[7], and the Beta VOC (also known as B.1.351), first identified in South Africa[8]. In spring 2021, Alpha rapidly became the prevailing variant in many regions of the world and a higher reproduction number was inferred from early epidemiological data[9–11]. In addition to the S^{D614G} change, Alpha has 18 different mutations in its genome, with two deletions and six substitutions within S alone[12]. Some of the S mutations, such as N501Y and H69-V70del, were hypothesized to confer enhanced replication and transmission capability, but clear experimental evidence is lacking[13,14]. Beta VOC has nine mutations in S, including N501Y and two in the S receptor-binding domain (RBD), K417N and E484K, the

[1]Institute of Diagnostic Virology, Friedrich-Loeffler-Institut, Greifswald-Insel, Riems, Germany. [2]Institute of Virology and Immunology, Mittelhäusern, Switzerland. [3]Department of Infectious Diseases and Pathobiology, Vetsuisse Faculty, University of Bern, Bern, Switzerland. [4]Institute of Veterinary Bacteriology, Vetsuisse Faculty, University of Bern, Bern, Switzerland. [5]Institute for Infectious Diseases, University of Bern, Bern, Switzerland. [6]CDC COVID-19 Emergency Response, Centers for Disease Control and Prevention, Atlanta, GA, USA. [7]Department of Microbiology and Molecular Medicine, Faculty of Medicine, University of Geneva, Geneva, Switzerland. [8]Charité – Universitätsmedizin Berlin, Institute of Virology, Berlin, Germany. [9]German Centre for Infection Research (DZIF), associated partner site Charité, Berlin, Germany. [10]Graduate School for Biomedical Science, University of Bern, Bern, Switzerland. [11]Department of Experimental Animal Facilities and Biorisk Management, Friedrich-Loeffler-Institut, Greifswald-Insel, Riems, Germany. [12]Centre for Vaccinology, Department of Pathology and Immunology, University of Geneva, Geneva, Switzerland. [13]Division of General Paediatrics, Department of Woman, Child and Adolescent Medicine, Faculty of Medicine, University of Geneva, Geneva, Switzerland. [14]Emory Vaccine Center, Emory University, Atlanta, GA, USA. [15]Division of Infectious Disease, Geneva University Hospitals, Geneva, Switzerland. [16]Division of Laboratory Medicine, Laboratory of Virology, Geneva University Hospitals, Geneva, Switzerland. [17]These authors contributed equally: Lorenz Ulrich, Nico Joel Halwe, Adriano Taddeo, Nadine Ebert. [18]These authors jointly supervised this work: Ronald Dijkman, Donata Hoffmann, Volker Thiel, Martin Beer, Charaf Benarafa. ✉e-mail: volker.thiel@vetsuisse.unibe.ch; martin.beer@fli.de; charaf.benarafa@vetsuisse.unibe.ch

latter putatively responsible for escaping neutralization from convalescent patient plasma[15–17]. Whether and which spike mutations are solely responsible for the putative fitness advantage is unknown.

Here, we investigated the fitness of the VOC Alpha or Beta compared to the predominant parental strain containing the S^{D614G} substitution – henceforth wt-S^{614G} – (i) in relevant primary airway culture systems *in vitro*, and (ii) in ferrets, Syrian hamsters, and two hACE2-expressing mouse models to assess specific advantages in replication and transmission and to evaluate the impact of Alpha S mutations alone *in vivo*. Neither Alpha nor Beta VOC showed enhanced replication in human airway epithelial cell (AEC) cultures compared to wt-S^{614G}. Competitive transmission experiments in Syrian hamsters demonstrated similar replication and transmission of wt-S^{614G} and Alpha, while both outcompeted Beta. However, competitive experiments in ferrets and transgenic mice expressing human angiotensin-converting enzyme 2 (hACE2) under the cytokeratin 18 promoter (hACE2-K18Tg), which overexpress hACE2 in epithelial cells, showed increased fitness of Alpha compared to wt-S^{614G}. Finally, Alpha and a recombinant clone expressing only the Alpha-specific spike mutations (wt-S^{Alpha}) both outcompeted the parental wt-S^{614G} strain with higher virus load in the upper respiratory tract of knock-in mice (hACE2-KI), expressing solely hACE2 in place of mouse ACE2. Like in AEC cultures, Beta showed lower fitness than w-S^{614G} in hACE2-KI mice. In all *in vivo* models, Alpha and wt-S^{614G} infections resulted in similar pathology.

Results

Binding and replication of VOCs in vitro

The evolution of SARS-CoV-2 variants is associated with accumulation of mutations in the spike (S) protein. The dissociation constant (K_D) between recombinant trimeric S of the VOC and immobilized dimeric human ACE2 (hACE2) was determined using Bio-layer interferometry. S^{Alpha} and S^{Beta} had a 4-fold higher affinity to hACE2 than S^{614G} (Extended Data Fig. 1a). Replication kinetics of Alpha, Beta, and a wild-type clinical isolate (with the S^{D614G} mutation) were comparable to each other in viral copies and titers in human primary nasal airway epithelial cell (AEC) cultures incubated at 33 and 37 °C (Extended Data Fig. 1b). However, in direct competition experiments in AEC cultures, Alpha had no advantage over wt-S^{614G}, while Beta was outcompeted by both Alpha and wt-S^{614G} (Extended Data Fig. 1c), indicating that competition experiments better expose replication differences between efficient variants.

Alpha and wt-S^{614G} on top in hamsters

Groups of six Syrian hamsters were each inoculated intranasally with a mixture of two SARS-CoV-2 strains comprising comparable genome equivalents in three one-to-one competition experiments: Alpha *vs* Beta, Beta *vs* wt-S^{614G}, and Alpha *vs* wt-S^{614G}. All experimentally infected "donor" hamsters were strictly kept in isolation cages to prevent intergroup spill-over infections. Each donor hamster was co-housed with a naïve "contact I" hamster 1 day post infection (dpi), creating six donor-contact I pairs to evaluate shedding and transmission. On 4 dpi, donor hamsters were euthanized, and six subsequent transmission pairs were set up by co-housing each contact I hamster with a naïve contact II hamster (Extended Data Fig. 2a).

In two competition experiments, wt-S^{614G} and Alpha outcompeted Beta in nasal washings of the donor hamsters from 1 dpi until euthanasia 4 dpi. Genome copies reached up to 10^9/mL for wt-S^{614G} and Alpha, whereas Beta viral loads were 10-fold lower at corresponding time points. Consequently, transmission of Beta was limited or undetectable in contact I and II hamsters compared to the competing variants wt-S^{614G} (Fig. 1) and Alpha (Extended Data Fig. 3). Transmission to contact animals was associated with clinical signs and weight loss (Extended Data Fig. 4a, b). In donor and contact hamsters, viral genome loads in the upper respiratory tract (URT: nasal conchae and trachea) revealed higher replication of Alpha and wt-S^{614G} as compared to Beta (Extended Data Figs. 5a, b), which can explain the lower transmission rate of Beta in a competition context. Of note, Beta replicated to high titers in the lower respiratory tract (LRT: cranial, medial, and caudal lung lobes) of donor hamsters, on par with the competing Alpha and wt-S^{614G} (Extended Data Figs. 5a, b).

In the Alpha vs wt-S^{614G} competition, no clear fitness difference was observed in virus replication in nasal washes of donor hamsters, and both variants were detected at all time-points in each donor with specific copies for each individual variant ranging from 10^5 to 10^9 genome copies/mL (Fig. 2). Of note, Alpha was dominant over wt-S^{614G} in the donor hamsters at 1 dpi, but ratios were balanced by the endpoint at 4 dpi. In organ samples of the donor hamsters, the highest viral loads were confirmed in the LRT, where Alpha was predominant (>66%) overall with over 10 times higher viral genome copies than wt-S^{614G} in 14 out of 18 lung samples from the 6 donor hamsters (Extended Data Fig. 5c). Sequential transmission to contact animals was associated with body weight loss (Extended Data Fig. 4c) and was highly efficient for both variants, which were simultaneously found in nasal washings of almost all contact I hamsters (Fig. 2). While all donor and contact I hamsters transmitted both viruses to their respective contacts, contact II hamsters principally shed one variant at high levels in nasal washes demonstrating comparable transmission ability for both variants. At the individual endpoints for contact I hamsters, Alpha appeared to dominate in the LRT when both variants were found at similar levels in the nasal washes and URT. In contact II, the principal variant in the URT was also found in the LRT (Extended Data Fig. 5c). High level SARS-CoV-2 replication in hamsters induced a rapid humoral immune response, as shown by serum reactivity in RBD-based ELISA in all but one contact hamsters (Extended Data Fig. 6a, b, c). In vitro, we measured a 2-fold increase in binding affinity of recombinant trimeric S^{Alpha} to hamster ACE2 compared to the affinity of S^{614G} (Extended Data Fig. 1d). These findings suggest that while S^{Alpha} has an increased binding affinity for ACE2, this factor was not predictive of the outcome of experimental infections in hamsters.

Alpha dominates over wt-S^{614G} in ferrets

In a similar approach as for hamsters, six donor ferrets were inoculated with a mixture of wt-S^{614G} and Alpha at comparable genome equivalents and sequential transmission was followed in naïve contact I and II ferrets (Extended Data Fig. 2b). Alpha rapidly became the dominant variant in nasal washings from 2 dpi with up to 10^5 viral genome copies per mL (Fig. 3). Correspondingly, the nasal concha of donor ferrets revealed high level replication in the nasal epithelium and up to 100-fold higher load of Alpha (up to $10^{8.2}$ viral genome copies per mL) than wt-S^{614G} (up to $10^{6.5}$ viral genome copies/ml) (Extended Data Fig. 7a). While histopathological analysis clearly indicated viral replication within the nasal epithelium of the donor ferrets (Extended Data Fig. 7b–e), no severe clinical signs were observed (Extended Data Fig. 4d, e). Transmission to contact I animals was only detected in two ferret pairs, from which only one contact I ferret transmitted the virus to the contact II ferret. However, in each of these three transmission events, the Alpha variant was vastly dominant and replicated to similarly high titers as in donor ferrets (Fig. 3). The 3 contact ferrets with virus shedding seroconverted by 15-20 days post contact (dpc) confirming active infection (Extended Data Fig. 6d).

Alpha overcomes wt-S^{614G} in K18Tg mice

To assess further adaptation of Alpha to human ACE2, four hACE2-K18Tg mice, which overexpress hACE2 in respiratory epithelium[18], were inoculated with a mixture of SARS-CoV-2 wt-S^{614G} and Alpha at comparable genome equivalents (Fig. 4a). Each inoculated mouse was co-housed with a contact hACE2-K18Tg mouse at 1 dpi. A complete predominance of Alpha in the oropharyngeal samples of all four inoculated mice was observed from 1 to 4 dpi with up to 10^6 viral genome copies/ml. The increased replicative fitness of Alpha over wt-S^{614G} was further reflected

throughout the respiratory tract with higher genome copies in nose, lungs, olfactory bulb, and brain at 4 dpi (Fig. 4a), and inoculated mice showed body weight loss at 4 dpi (Extended Data Fig. 8a). A relatively high infectious dose was used to promote transmission and was associated with high virus load (up to 10^8 viral genome copies per sample) in the lung and brain leading to encephalitis as previously reported in hACE2-K18Tg mice[19,20]. In the nose and oropharyngeal swabs, viral loads were relatively lower and only limited transmission was observed (2 out of 4 contact). None of the contact mice lost weight, yet only Alpha was detectable in the lungs of contact mice 7 dpc (Extended Data Fig. 8b).

A similar competition experiment was performed between wt-S^{614G} and wt-S^{Alpha}, an isogenic recombinant virus expressing S^{Alpha}. hACE2-K18Tg mice were inoculated with an equal mixture of wt-S^{Alpha} and wt-S^{614G} and placed with a contact hACE2-K18Tg mouse at 1 dpi. Interestingly, the replicative advantage of wt-S^{Alpha} was less clear, where both wt-S^{Alpha} and wt-S^{614G} showed comparably high viral genome copies in lung and brain samples (Fig. 4b). Transmission to contact mice was inefficient, yet again wt-S^{Alpha} was the only virus detected in lungs of contact mice 7 dpc (Extended Data Fig. 8b). The results indicate that the S^{Alpha} spike mutations contribute partly to the replication advantage of Alpha over wt-S^{614G} in the URT of mice that express high levels of hACE2.

Alpha > wt-S^{614G} > Beta in hACE2-KI mice

To further address this question, we next used hACE2-KI homozygous mice, which express hACE2 in place of mouse ACE2 under the endogenous mouse *Ace2* promoter[3]. In contrast to hACE2-K18Tg mice, hACE2-KI mice have a physiological expression of hACE2 with no ectopic expression of hACE2 in the brain, and no expression of mouse ACE2, which has been shown to be permissive to the spike mutation N501Y contained in S^{Alpha}. Four groups of hACE2-KI mice were inoculated intranasally with 10^4 PFU/mouse of either SARS-CoV-2 wt-S^{614G}, Alpha, wt-S^{Alpha}, or Beta (n=8/group) as individual virus infections. Significantly higher viral genome copy numbers were observed in mice infected with Alpha, wt-S^{Alpha}, or Beta compared to wt-S^{614G} in oropharyngeal swabs 1 dpi (Extended Data Fig. 9a). Moreover, significantly higher viral genome copies of Alpha and wt-S^{Alpha} were observed in the nose 2 dpi, and olfactory bulb 4 dpi compared to wt-S^{614G} and Beta (Extended Data Fig. 9b). Of note, virus titers in the nasal airways and lungs showed SARS-CoV-2 persistence 4 dpi in 3 out of 4 mice infected either with Alpha or with wt-S^{Alpha}, but not for mice inoculated with wt-S^{614G}, while Beta persisted only in the lung of two out of four mice (Extended Data Fig. 9c). The apparent discrepancy between genome copies and PFUs reflect the non-homogeneous distribution of the virus in the different samples processed for each assay. No difference in weight loss (Extended Data Fig. 9d) or lung histopathology score (SI Table 1) was observed between groups.

Finally, we performed competition experiments to compare the replication of the VOC in groups of hACE2-KI mice. We observed a complete predominance of Alpha and wt-S^{Alpha} over wt-S^{614G} (Fig. 5a-c). In contrast, Beta showed reduced fitness compared to wt-S^{614G} (Fig. 5d). Together, the two mouse models support enhanced fitness of SARS-CoV-2 Alpha VOC over its ancestor wt-S^{614G} with increased replication and persistence in the URT and better systemic spread, mediated in part by changes located within the Alpha spike sequence.

Discussion

Fitness of Alpha in restrictive models

Epidemiological data indicate that new SARS-CoV-2 variant lineages with specific amino acid changes have a fitness advantage over contemporary strains. VOC such as Alpha and Beta are particularly concerning for their hypothesized ability to supersede progenitor strains and establish immune escape properties, respectively. In this comprehensive study, we provide experimental evidence that SARS-CoV-2 Alpha has a clear replication advantage over wt-S^{614G} in both ferret and two humanized mouse models. Moreover, Alpha exclusively was transmitted to contact animals in competition experiments, where ferrets and hACE2-K18Tg mice were inoculated with mixtures of Alpha and wt-S^{614G}. Because SARS-CoV-2 replicates to lower levels in ferrets and hACE2-KI mice, the absence of detection of wt-S^{614G} in some samples of inoculated animals reflects also the limit of detection of the RT-PCR assays ($\alpha 10^3$ genome copies/ml).

We have shown that the molecular mechanism behind the fitness advantage of Alpha *in vivo* is largely dependent on a few changes in S including three amino acid deletions (H69, V70, Y144) and six substitutions (N501Y, A570D, P681H, T716I, S982A, D1118H). In hACE2-KI mice, higher genome copies and/or titers of Alpha and wt-S^{Alpha} compared to wt-S^{614G} were found in the URT (oropharynx, nose) and olfactory bulb. Increased replication and transmission of wt-S^{Alpha} over wt-S^{614G} were also evident in hACE2-K18Tg mice. Transmission events are rare in mice, however, we observed transmission of Alpha and wt-S^{Alpha} in 50% of the contact hACE2-K18Tg mice and no detection of wt-S^{614G} in any contact mouse. *In vitro*, Alpha spike mutations increased its affinity 2 to 4-fold to hamster and human ACE2, respectively, indicating an overall improvement in binding abilities rather than a specialization to human ACE2.

Beta is outcompeted in vitro and in vivo

Beta showed a higher binding affinity for human ACE2 than its progenitor wt-S^{614G} and an equally strong replication as Alpha and wt-S^{614G} in single infections of AEC cultures and in hACE2-KI mice. However, Beta replication was outcompeted in direct competitions with wt-S^{614G} in vitro and in hACE2-KI mice. In hamsters, wt-S^{614G} and Alpha also fully outcompeted Beta in replication and in transmission to contact animals, where Beta was in the minority by one or two orders of magnitude. This reduced fitness was also evident in previous experiments in K18-hACE2 mice[21]. The relative reduced intrinsic fitness of Beta in immunologically naïve hosts supports the hypothesis that the epidemiological advantage of Beta may principally be due to immune escape as indicated by reduced efficiency in serum neutralization tests[16]. In immune –convalescent or vaccinated– populations, the immune escape advantage of Beta may prove to be sufficient to compensate for the intrinsic reduced fitness and explains e.g., the low prevalence of this variant in regions with a mainly naïve population.

Alpha and wt-S^{614G} thrive in hamsters

Alpha and wt-S^{614G} were comparable in their replication and transmission in hamsters, a model with very high susceptibility and replication efficacy where the impact of a marginally fitter SARS-CoV-2 variant may not become apparent. Indeed, efficient simultaneous transmission of both variants to contact hamsters was observed in association with high viral loads in infected animals. In models supporting high replication, such as human AEC cultures and hamsters, only major improvement in replication and transmission can be detected when the variants compared already have a very high fitness. In contrast, in ferrets and mice as animal models where SARS-CoV-2 replication is overall less efficient, VOC with a modest, but real ability for improved replication and transmission can be identified. The similar replication and transmission efficacy in hamsters are also in line with recent publications using the hamster model and VOC[22].

The basal rate of replication is an important factor in the assertion of a variant over a contemporary variant in a naïve population. Some individuals with higher bioaerosol exhalation levels can initiate disproportionate numbers of transmission events, possibly because of higher viral load in the URT, and are therefore called "superspreaders"[23]. The hamster model might thus resemble the human superspreader scenario, since there is no clear indication of a specific predominance in transmission between two SARS-CoV-2 variants with high fitness levels, such as wt-S^{614G} and Alpha. However, we did not perform strict aerosol transmission studies, so we can only partially conclude on

the superspreader aspects of the model. In the ferret and hACE2-KI models, more restrictions are found, e.g., to the URT. Therefore, these models more closely mimic the situation in humans with a dominance of mild infections. While the transmission events were not high overall (3 out of 8 pairs in ferrets, and 4 out of 8 in hACE2-K18Tg mice), the almost exclusive transmission of Alpha relative to wt-S^{614G} mirrored the higher transmission rate in the human population to some extent, where Alpha has been responsible for more than 90% of infections in most countries in Europe[24].

Overall, our study demonstrates that multiple complementary models are necessary to comprehensively evaluate different aspects of human SARS-CoV-2 infection and the impact of emerging VOC on the course of the ongoing pandemic. The hamster and ferret models are complementary models for transmission efficiency. The mouse models used here may become critical for VOC demonstrating higher specificity for binding hACE2 relative to other species. The combined analysis of our results allows a clear conclusion supporting a fitness advantage of Alpha and a concomitant disadvantage of Beta, which is in line with the observed epidemiological predominance of Alpha in the context of a fairly naïve population. Importantly, and reassuringly, despite the apparent fitness differences of these VOC, there is no indication of increased pathology.

Online content

Any methods, additional references, Nature Research reporting summaries, source data, extended data, supplementary information, acknowledgements, peer review information; details of author contributions and competing interests; and statements of data and code availability are available at https://doi.org/10.1038/s41586-021-04342-0.

1. Harvey, W. T. et al. SARS-CoV-2 variants, spike mutations and immune escape. *Nat Rev Microbiol* **19**, 409-424, https://doi.org/10.1038/s41579-021-00573-0 (2021).
2. Tao, K. et al. The biological and clinical significance of emerging SARS-CoV-2 variants. *Nat Rev Genet* **22**, 757-773, https://doi.org/10.1038/s41576-021-00408-x (2021).
3. Zhou, B. et al. SARS-CoV-2 spike D614G change enhances replication and transmission. *Nature* **592**, 122-127, https://doi.org/10.1038/s41586-021-03361-1 (2021).
4. Korber, B. et al. Tracking Changes in SARS-CoV-2 Spike: Evidence that D614G Increases Infectivity of the COVID-19 Virus. *Cell* **182**, 812-827 e819, https://doi.org/10.1016/j.cell.2020.06.043 (2020).
5. Plante, J. A. et al. Spike mutation D614G alters SARS-CoV-2 fitness. *Nature* **592**, 116-121, https://doi.org/10.1038/s41586-020-2895-3 (2021).
6. Hou, Y. J. et al. SARS-CoV-2 D614G variant exhibits efficient replication ex vivo and transmission in vivo. *Science* **370**, 1464-1468, https://doi.org/10.1126/science.abe8499 (2020).
7. Volz, E. et al. Assessing transmissibility of SARS-CoV-2 lineage B.1.1.7 in England. *Nature* **593**, 266-269, https://doi.org/10.1038/s41586-021-03470-x (2021).
8. Tegally, H. et al. Detection of a SARS-CoV-2 variant of concern in South Africa. *Nature* **592**, 438-443, https://doi.org/10.1038/s41586-021-03402-9 (2021).
9. Davies, N. G. et al. Estimated transmissibility and impact of SARS-CoV-2 lineage B.1.1.7 in England. *Science* **372**, https://doi.org/10.1126/science.abg3055 (2021).
10. Washington, N. L. et al. Emergence and rapid transmission of SARS-CoV-2 B.1.1.7 in the United States. *Cell* **184**, 2587-2594 e2587, https://doi.org/10.1016/j.cell.2021.03.052 (2021).
11. Weber, S., Ramirez, C. M., Weiser, B., Burger, H. & Doerfler, W. SARS-CoV-2 worldwide replication drives rapid rise and selection of mutations across the viral genome: a time-course study - potential challenge for vaccines and therapies. *EMBO Mol Med*, e14062, https://doi.org/10.15252/emmm.202114062 (2021).
12. Galloway, S. E. et al. Emergence of SARS-CoV-2 B.1.1.7 Lineage - United States, December 29, 2020-January 12, 2021. *MMWR Morb Mortal Wkly Rep* **70**, 95-99, https://doi.org/10.15585/mmwr.mm7003e2 (2021).
13. Liu, Y. et al. The N501Y spike substitution enhances SARS-CoV-2 transmission. *bioRxiv*,https://doi.org/10.1101/2021.03.08.434499 (2021).
14. Kemp, S. et al. Recurrent emergence and transmission of a SARS-CoV-2 Spike deletion H69/V70. *bioRxiv*, 2020.2012.2014.422555, https://doi.org/10.1101/2020.12.14.422555 (2021).
15. Cele, S. et al. Escape of SARS-CoV-2 501Y.V2 from neutralization by convalescent plasma. *Nature* **593**, 142-146, https://doi.org/10.1038/s41586-021-03471-w (2021).
16. Hoffmann, M. et al. SARS-CoV-2 variants B.1.351 and P.1 escape from neutralizing antibodies. *Cell* **184**, 2384-2393 e2312, https://doi.org/10.1016/j.cell.2021.03.036 (2021).
17. Wibmer, C. K. et al. SARS-CoV-2 501Y.V2 escapes neutralization by South African COVID-19 donor plasma. *Nat Med* **27**, 622-625, https://doi.org/10.1038/s41591-021-01285-x (2021).
18. McCray, P. B., Jr et al. Lethal infection of K18-hACE2 mice infected with severe acute respiratory syndrome coronavirus. *J Virol* **81**, 813-821, https://doi.org/10.1128/JVI.02012-06 (2007).
19. Yinda, C. K. et al. K18-hACE2 mice develop respiratory disease resembling severe COVID-19. *PLoS Pathog* **17**, e1009195, https://doi.org/10.1371/journal.ppat.1009195 (2021).
20. Zheng, J. et al. COVID-19 treatments and pathogenesis including anosmia in K18-hACE2 mice. *Nature* **589**, 603-607, https://doi.org/10.1038/s41586-020-2943-z (2021).
21. Hoffmann, D. et al. CVnCoV and CV2CoV protect human ACE2 transgenic mice from ancestral B BavPat1 and emerging B.1.351 SARS-CoV-2. *Nat Commun* **12**, 4048, https://doi.org/10.1038/s41467-021-24339-7 (2021).
22. Abdelnabi, R. et al. Comparing infectivity and virulence of emerging SARS-CoV-2 variants in Syrian hamsters. *EBioMedicine* **68**, 103403, https://doi.org/10.1016/j.ebiom.2021.103403 (2021).
23. Edwards, D. A. et al. Exhaled aerosol increases with COVID-19 infection, age, and obesity. *Proc Natl Acad Sci U S A* **118**, https://doi.org/10.1073/pnas.2021830118 (2021).
24. https://www.ecdc.europa.eu/en/covid-19/variants-concern. *ECDC*, <https://www.ecdc.europa.eu/en/covid-19/variants-concern> (June 3rd, 2021).

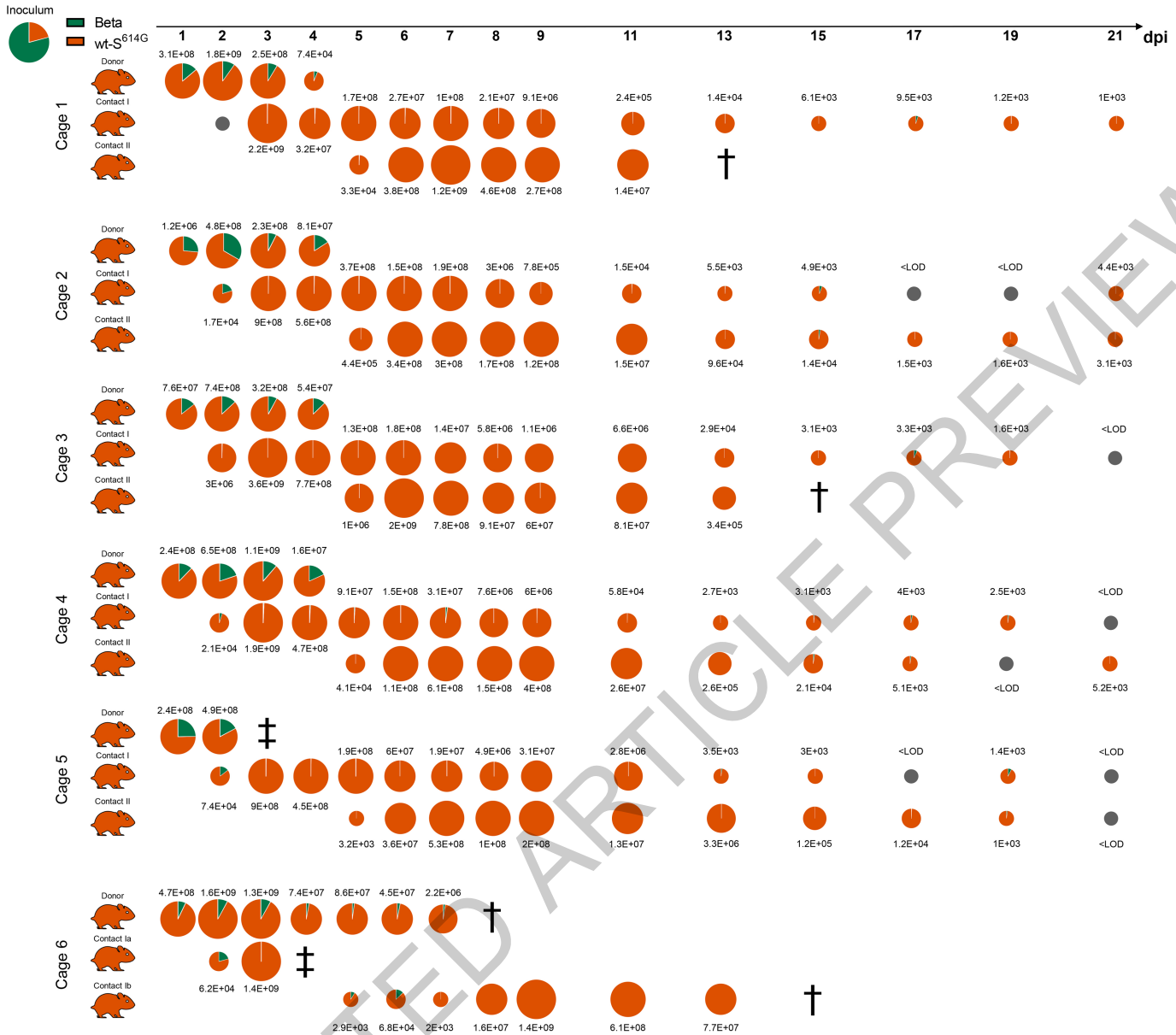

Fig. 1 | Competitive replication and transmission of Beta and wt-S^{614G} in Syrian hamsters. Six donor hamsters were each inoculated with $10^{4.25}$ $TCID_{50}$ determined by back titration and composed of a mixture of wt-S^{614G} (orange) and Beta (green) at 1:3.8 ratio determined by RT-qPCR. Donor hamsters, contact I and II hamsters were co-housed sequentially as shown in Extended Data Fig. 2a. Nasal washings were performed daily from 1-9 dpi and afterwards every two days until 21 dpi. Pie chart colors illustrate the ratio of variants detected in nasal washings at the indicated day post inoculation (dpi). Pie chart sizes are proportional to the total viral genome copies reported above or below respective pies. Grey pies indicate values below the limit of detection (LOD, $<10^3$ viral genome copies per sample). Hamster silhouettes are colored according to the dominant variant (>66%) detected in the latest positive sample of each animal. † indicate that the corresponding animal reached the humane endpoint. ‡ indicate hamsters that passed away during inhalation anesthesia on 3 and 4 dpi. This required changes in the group composition in cage 6, where the donor hamster was kept until 7 dpi and was co-housed in two different pairs: donor – contact Ia pair and another donor – contact Ib pair.

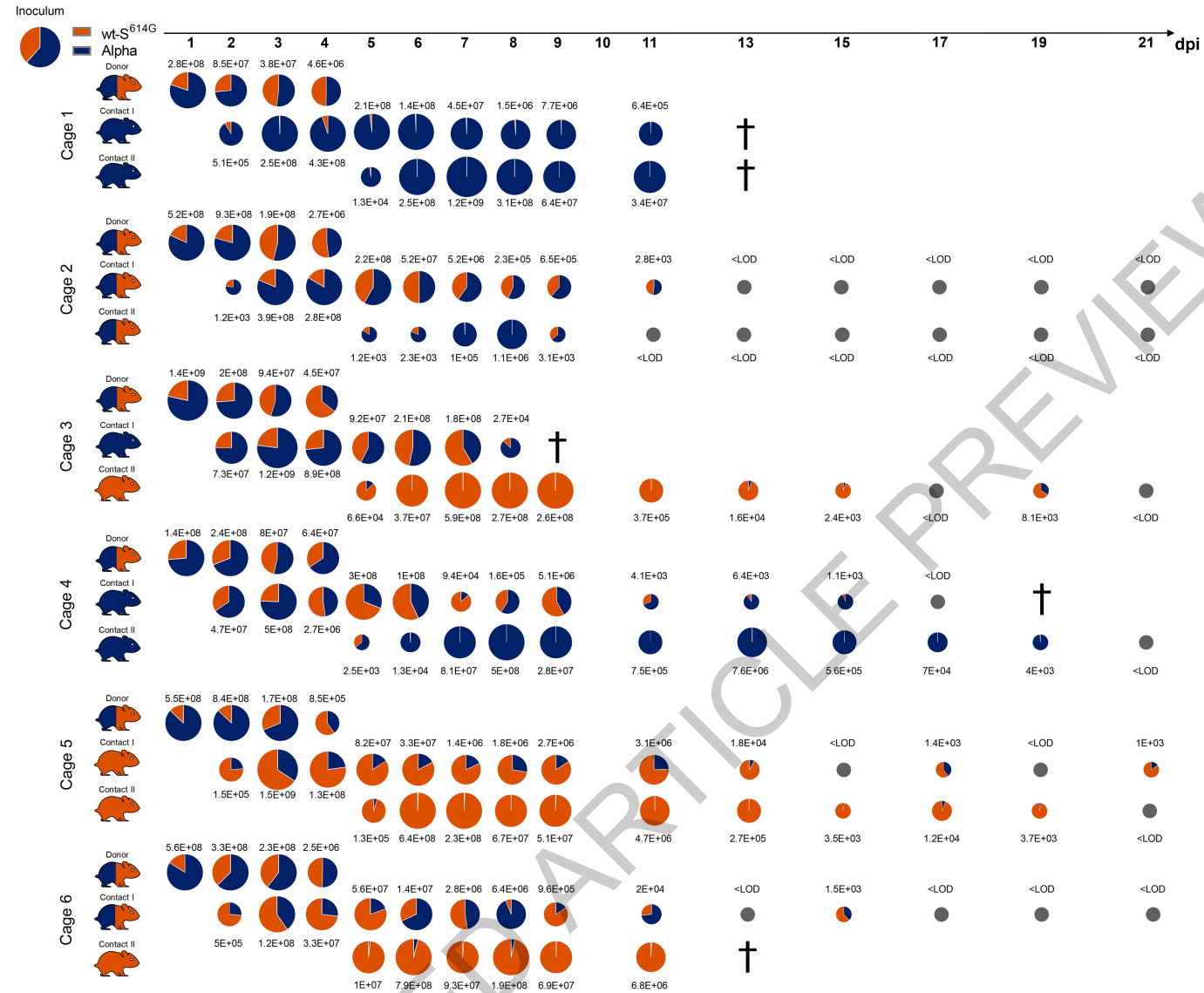

Fig. 2 | Competitive replication and transmission of Alpha and wt-S^{614G} in Syrian hamsters. Six donor hamsters were each inoculated with $10^{4.3}$ $TCID_{50}$ determined by back titration and composed of a mixture of wt-S^{614G} and Alpha at 1:1.6 ratio determined by RT-qPCR. Donor hamsters, contact I and II hamsters were co-housed sequentially as shown in Extended Data Fig. 2a. Nasal washings were performed daily from 1-9 dpi and afterwards every two days until 21 dpi. Pie chart colors illustrate the ratio of variants detected in nasal washings at the indicated dpi. Pie chart sizes are proportional to the total viral genome copies reported above or below respective pies. Grey pies indicate values below the LOD (<10^3 viral genome copies per sample). Hamster silhouettes are colored according to the dominant variant (>66%) detected in the latest positive sample of each animal; bi-coloring indicates no dominance of a single variant. † indicate that the corresponding animal reached the humane endpoint.

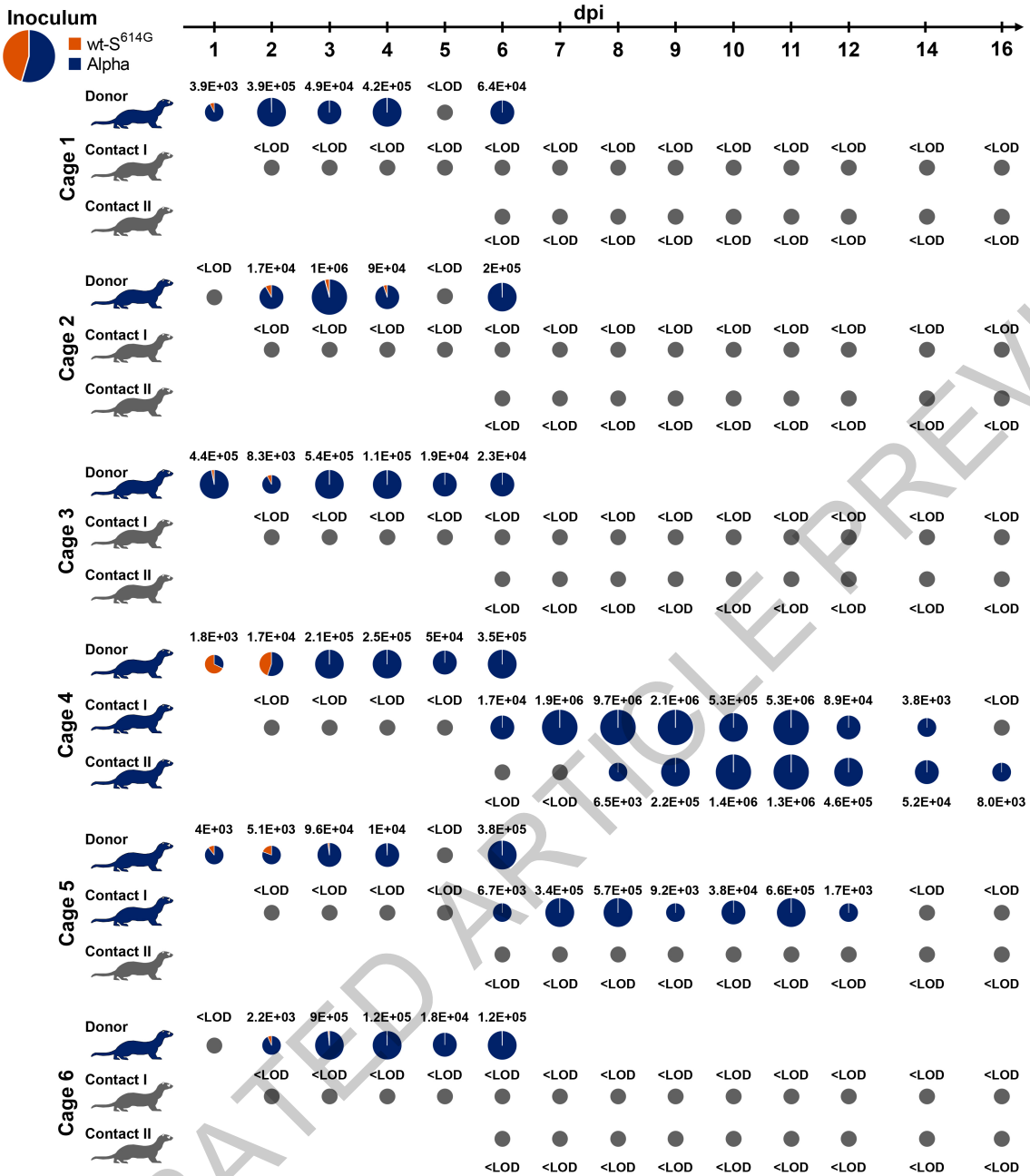

Fig. 3 | Replication and transmission of SARS-CoV-2 Alpha and wt-S^{614G} in ferrets. Six donor ferrets were each inoculated with $10^{5.9}$ $TCID_{50}$ determined by back titration and composed of a mixture of wt-S^{614G} and Alpha at 1:1.2 ratio determined by RT-qPCR. Donor ferrets, contact I and II ferrets were co-housed sequentially as shown in Extended Data Fig. 2b. Pie chart colors illustrate the ratio of variants detected in nasal washings at the indicated dpi. Pie chart sizes are proportional to the total viral genome copies reported above or below respective pies. Grey pies indicate values below the LOD (<10^3 viral genome copies per sample). Viral genome copies were <LOD on 18 and 20 dpi (not shown). Coloring of the ferret silhouettes refers to the predominant SARS-CoV-2 variant (>66%) detected in the latest positive sample of the corresponding animal.

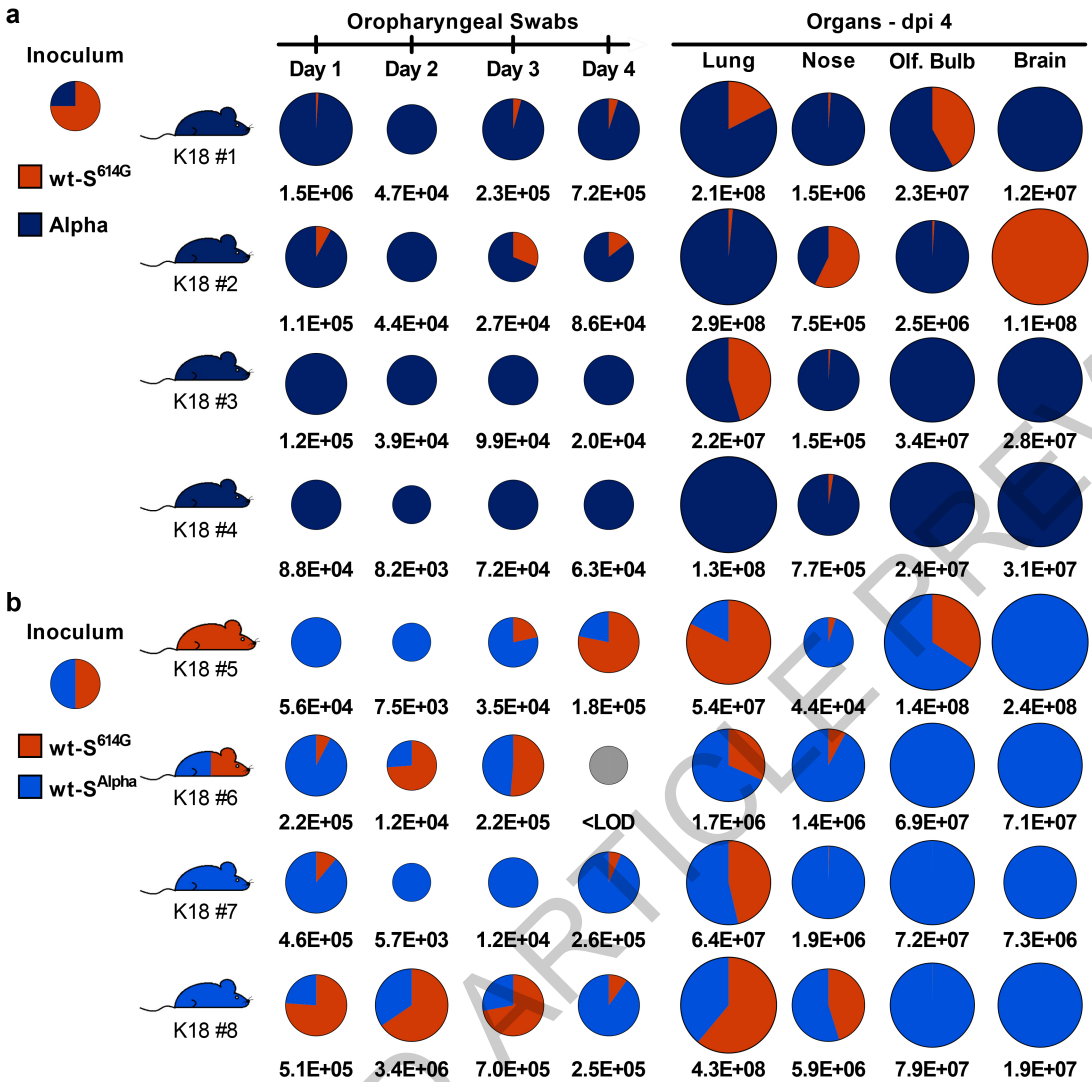

Fig. 4 | Replication of Alpha, wt-S^{Alpha}, and wt-S^{614G} in hACE2-K18Tg mice. Two groups of four donor hACE2-K18Tg mice were inoculated with 1x10^4 PFU determined by back titration and composed of (a) a mixture of wt-S^{614G} (orange) and Alpha (dark blue) at 3:1 ratio, and (b) a mixture of wt-S^{614G} and wt-S^{Alpha} (light blue) at 1:1 ratio. Pie chart colors illustrate the ratio of variants detected in each sample at the indicated dpi. Pie chart sizes are proportional to the total viral genome copies reported below. Grey pies indicate values below the LOD (<10^3 viral genome copies per sample). Coloring of the mouse silhouettes corresponds to the predominant SARS-CoV-2 variant (>66%) in the latest positive swab sample of the corresponding mouse; bi-coloring indicates no dominance of a single variant. K18 #1 to #8 denote individual hACE-K18Tg donor mice.

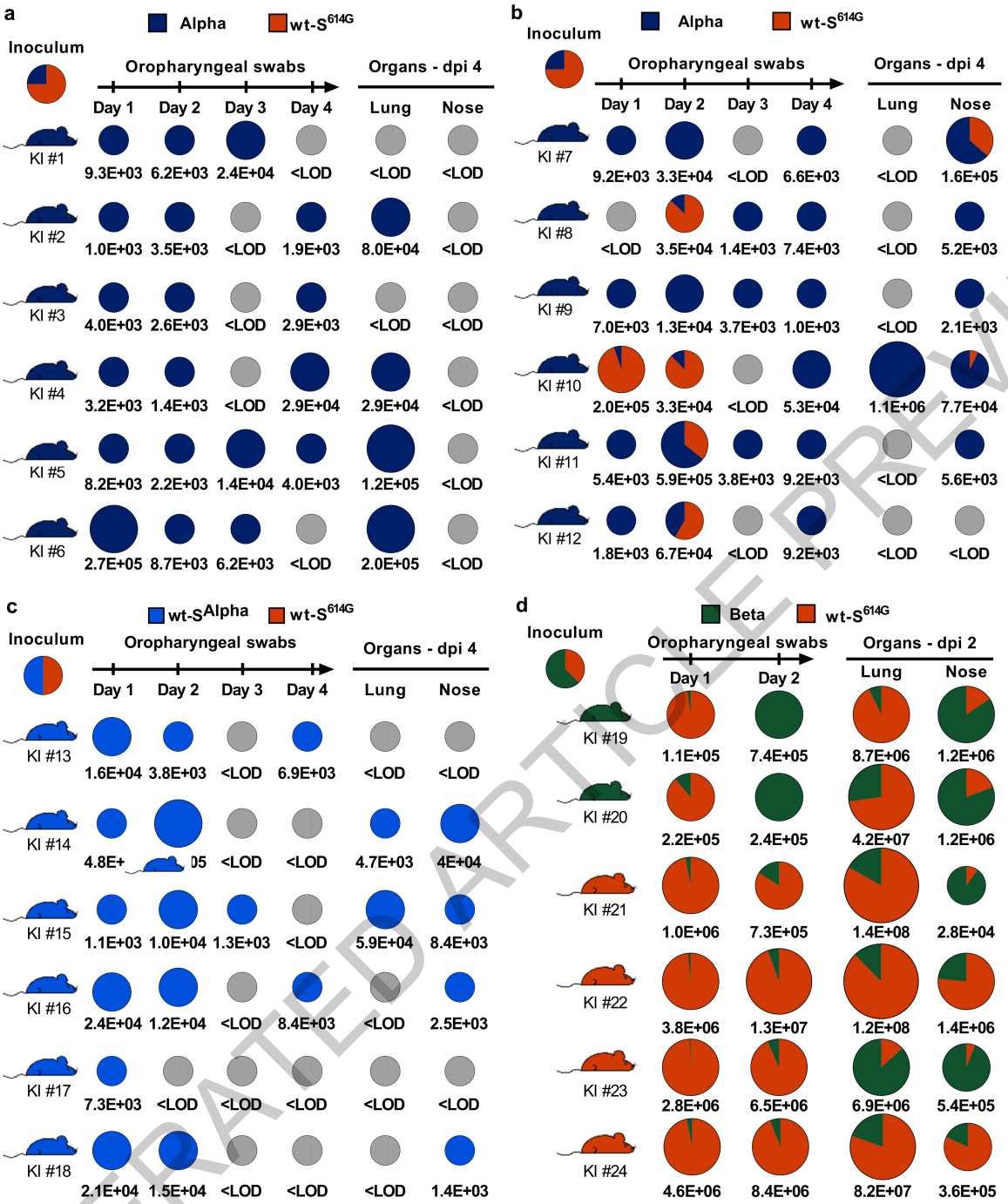

Fig. 5 | Replication of Alpha, wt-S^{Alpha}, and Beta in competition with wt-S^{614G} in hACE2-KI mice. Groups of hACE2-KI male (a, c, d) and female (b) mice were inoculated with 1x10^4 PFU determined by back titration and composed of (a, b) a mixture of wt-S^{614G} and Alpha at 3:1 ratio, (c) a mixture of wt-S^{614G} and wt-S^{Alpha} at 1:1 ratio, and (d) a mixture of wt-S^{614G} and Beta 1:1.6 ratio. Pie chart colors illustrate the ratio of variants detected in each sample at the indicated dpi. Pie chart sizes are proportional to the total viral genome copies reported below. Grey pies indicate values below the LOD (<10^3 viral genome copies per sample). Coloring of the mouse silhouettes corresponds to the predominant SARS-CoV-2 variant (>66%) in the latest positive swab sample of the corresponding mouse. KI#1-24 denote individual hACE2-KI mice.

Methods

Cell lines

Vero E6 cells (ATCC CRL-1586) (kindly provided by Doreen Muth, Marcel Müller, and Christian Drosten, Charité, Berlin, Germany) or Vero-TMPRSS2[25] (kindly provided by Stefan Pöhlmann, German Primate Center - Leibniz Institute for Primate Research, Göttingen, Germany) were propagated in Dulbecco's Modified Eagle Medium-GlutaMAX™ supplemented with 1 mM sodium pyruvate, 10% (v/v) heat-inactivated fetal bovine serum (FBS), 100 µg/ml streptomycin, 100 IU/ml penicillin, 1% (w/v) nonessential amino acids, and 15 mM HEPES (Gibco, Gaithersburg, Maryland, United States of America). Cells were maintained at 37 °C in a humidified incubator with 5% CO_2.

Viruses

Viruses are listed in Extended Data Table 1 together with the corresponding *in vitro* and *in vivo* experiments in which they were used. Specific amino acid changes are shown schematically in Extended Data Fig. 10. Contemporary clinical isolates from the B.1.160 (S^{D614G}) (EPI_ISL_414019), Alpha (EPI_ISL_2131446, EPI_ISL_751799 (L4549)) and Beta (EPI_ISL_803957 (L4550)) were isolated and minimal passaged upon Vero E6 cells. Beta (EPI_ISL_981782) was initially isolated on A549 cells expressing hACE2 before passaging on Vero E6 cells. SARS-CoV-2 Alpha (L4549) and Beta (L4550)[21] were received from the Robert-Koch-Institut Berlin, Germany. Isogenic variants with the Alpha spike (wt-S^{Alpha}) or individual Alpha spike mutations were introduced into a wild-type SARS-COV-2 "Wuhan" backbone strain comprising the D614G amino acid change (wt-S^{614G}), as described previously[3,26]. Isogenic viruses were grown on Vero-TMPRSS2 cells, after one passage on human bronchial airway epithelial cells. All viruses were verified by performing whole-genome NGS sequencing (see below). For SARS-CoV-2 Alpha (L4549, SARS-CoV-2 B.1.1.7 NW-RKI-I-0026/2020 passage 3), one silent mutation in the ORF1a (sequence position 11741) was determined (C to T with 27% T, 57% strand bias). For SARS-CoV-2 Beta (L4550, available under ENA study accession number MZ433432), one nucleotide exchange was detected (A12042C) resulting in the amino acid exchange D3926A in ORF1a and one SNP at sequence position 11730 (C to T with 41%, stand bias 52%).

For all *in vivo* virus competition experiments, we generated inoculum mixtures aiming for a 1:1 ratio of each variant based on virus stock titers. The reported mixture inoculum titers are based on back-titration of the inoculum mixtures and the indicated ratio of each variant was determined by the standard RT-qPCR. SARS-CoV-2 wt-S^{614G} (PRJEB45736; wt-S614G ID#49 vial 2) and SARS-CoV-2 Beta (L4550) were used to inoculate hamsters in the wt-S^{614G} vs. Beta study; SARS-CoV-2 Alpha (L4549), and SARS-CoV-2 Beta (L4550) were used for inoculation in the Alpha vs. Beta hamster study. SARS-CoV-2 wt-S^{614G}, wt-S^{Alpha}, Alpha (L4549), and Beta (L4550) were used to inoculate hACE2 humanized mice in all single virus or mixed virus competition experiments.

Next-generation sequencing (NGS)

NGS was used to verify the sequence of isolates and isogenic clones prior to experimentation. RNA was extracted using the RNAdvance Tissue kit (Beckman Coulter) and the KingFisher Flex System (Thermo Fisher Scientific). Subsequently, RNA was transcribed into cDNA and sequencing libraries were generated as described[27] and were sequenced using the Ion Torrent S5XL Instrument (ThermoFisher). Samples with Ct values >20 for SARS-CoV-2 were additionally treated with RNA baits (myBaits, Arbor Biosciences) for SARS-CoV-2 enrichment before sequencing[28]. Sequence datasets were analyzed via reference mapping with the Genome Sequencer Software Suite (version 2.6; Roche, https://roche.com), default software settings for quality filtering and mapping using EPI_ISL_414019 (Alpha), EPI_ISL_2131446 (Alpha) and EPI_ISL_981782 (Beta) as references. To identify potential single nucleotide polymorphisms in the read data, the variant analysis tool integrated in Geneious Prime (2019.2.3) was applied (default settings).

Primary human nasal airway epithelial cell (AEC) cultures

Human nasal AEC cultures were purchased from Epithelix SARL, Geneva, (EP02MP Nasal MucilAir™ Pool of 14 Donors). Maintenance of primary nasal AEC cultures were performed according to manufacturer's guidelines. Individual SARS-CoV-2 infections with contemporary virus isolates were conducted at either 33 °C or 37 °C as described elsewhere using an MOI of 0.02[29], while all competition experiments and replication kinetics were performed with an MOI of 0.005 as described previously[30]. The viral load quantification of individual SARS-CoV-2 infections with contemporary virus isolates was performed using the NucliSens easyMAG (BioMérieux) and quantitative real-time PCR (RT-qPCR) targeting the E gene of SARS-CoV-2 as described[31,32]. The competition experiments nucleic acids were extracted using the Quick-RNA Viral 96 kit (Zymo research) and the RT-qPCR primers and probe sequences are shown in Extended Data Table 2. The viral replication of individual isogenic variants was monitored via plaque assay.

Plaque titration assay

Viruses released into the apical compartments were titrated by plaque assay on Vero E6 cells, as previously described[30,33]. Briefly, 2x10^5 cells/ml were seeded in 24-well plates 1 day prior to titration and inoculated with 10-fold serial dilutions of virus solutions. Inoculums were removed 1 hour post-infection and replaced with overlay medium consisting of DMEM supplemented with 1.2% Avicel (RC-581, FMC biopolymer), 15 mM HEPES, 5 or 10% heat-inactivated FBS, 100 µg/ml streptomycin, and 100 IU/ml penicillin. Cells were incubated at 37 °C, 5% CO_2 for 48 hours, fixed with 4% (v/v) neutral buffered formalin, and stained with crystal violet.

Protein expression, purification, and biolayer interferometry assay

SARS-CoV-2 spike protein expression plasmids were constructed to encode the ectodomain of spike protein S^{614G} or S^{Alpha} (residues 1–1208, with a mutated furin cleavage site and K986P/V987P substitutions) followed by a T4 foldon trimerization domain and a polyhistidine purification tag. ACE2 protein (human, hamster, or ferret) expression plasmids were constructed to encode the ectodomain of ACE2 followed by a human IgG1 Fc purification tag. The recombinant proteins were expressed using the Expi293 Expression system (ThermoFisher Scientific) and purified with HisTrap FF columns (for polyhistidine-tagged spike proteins) or with HiTrap Protein A column (for Fc-tagged ACE2 proteins) in FPLC (Cytiva) system. Recombinant proteins were further purified with Superose 6 Increase 10/300 GL column (Cytiva) as needed.

Binding affinity between the trimeric spike and dimeric ACE2 were evaluated using Octet RED96e instrument at 30 °C with a shaking speed at 1000 RPM (ForteBio). Anti-human IgG Fc biosensors (ForteBio) were used. Following 20 minutes of pre-hydration of anti-human IgG Fc biosensors and 1 minute of sensor check, 7.5 nM of human ACE2-Fc, 7.5 nM of hamster ACE2-Fc, or 10 nM of ferret ACE2-Fc in 10X kinetic buffer (ForteBio) were loaded onto the surface of anti-human IgG Fc biosensors for 5 minutes. After 1.5 minutes of baseline equilibration, 5 minutes of association was conducted at 10 – 100 nM S^{614G}, S^{Alpha} or S^{Beta}, for human or hamster ACE2-Fc, followed by 5 minutes of dissociation in the same buffer, which was used for baseline equilibration. For binding assays using ferret ACE2-Fc, association was conducted with 25 – 200 nM S^{614G} or S^{Alpha}. The data were collected using ForteBio Data Acquisition Software 12.0.1 and corrected by subtracting signal from the reference sample and a 1:1 binding model with global fit was used for determination of affinity constants.

Animal experimentation ethics declarations

All ferret and hamster experiments were evaluated by the responsible ethics committee of the State Office of Agriculture, Food Safety, and

Fishery in Mecklenburg–Western Pomerania (LALLF M-V) and gained governmental approval under registration number LVL MV TSD/7221.3-1-004/21. Mouse studies were approved by the Commission for Animal Experimentation of the Cantonal Veterinary Office of Bern and conducted in compliance with the Swiss Animal Welfare legislation and under license BE-43/20.

Hamster studies

Six Syrian hamsters (*Mesocricetus auratus*) (Janvier Labs) were inoculated intranasally under a brief inhalation anesthesia with a 70µl mixture of two respective SARS-CoV-2 VOC (wt-S^{614G} vs. Alpha mixture, wt-S^{614G} vs. Beta mixture, and Alpha vs. Beta mixture). Each inoculum was back-titrated and ratios of each variant were determined by RT-qPCR. The wt-S^{614G} and Alpha mixture held a 1:1.6 ratio with $10^{4.3}$ $TCID_{50}$ per hamster, the wt-S^{614G} vs. Beta mixture held a 1:3.8 ratio with $10^{4.25}$ $TCID_{50}$ per hamster, and the Alpha vs. Beta mixture held a 1.8:1 ratio with $10^{5.06}$ $TCID_{50}$ per hamster.

Inoculated donor hamsters were isolated in individually ventilated cages for 24 hours. Thereafter, contact hamster I was co-housed to each donor, creating six donor-contact I pairs (Extended Data Fig. 2a). The housing of each hamster pair was strictly separated in individual cage systems to prevent spillover between different pairs. Four days post inoculation (dpi), the individual donor hamsters (inoculated animal) were euthanized. To simulate a second transmission cycle, the original contact hamsters (referred to as contact I) were commingled with a further six naïve hamsters (referred to as contact II), which equates to another six contact I and contact II pairs (Extended Data Fig. 2a). These pairs were co-housed until the end of the study at 21 dpi. Because the first contact hamster (cage 6) in the competition trial wt-S^{614G} vs. Alpha, died already 2 dpc, the second contact hamster for this cage was also co-housed with the donor hamster; thus the first and second contact hamsters in this cage were labeled contact Ia and contact Ib, respectively. To enable sufficient contact between the donor hamster and contact Ib hamster, which was commingled routinely on 4 dpi, the donor hamster was euthanized not before 7 dpi (instead of 4 dpi), when it finally reached the humane end-point criterion for bodyweight (below 80% of 0 dpi body weight).

Viral shedding was monitored by nasal washings in addition to a daily physical examination and body weighing routine. Nasal washing samples were obtained under a short-term isoflurane anesthesia from individual hamsters by administering 200µl PBS to each nostril and collecting the reflux. Animals were sampled daily from 1 dpi to 9 dpi, and afterwards, every other day until 21 dpi. Under euthanasia, serum samples and an organ panel comprising representative upper (URT) and lower respiratory tract (LRT) tissues were collected from each hamster. All animals were observed daily for signs of clinical disease and weight loss. Animals reaching the humane endpoint, e.g., falling below 80% of the initial body weight relative to 0 dpi, were humanely euthanized.

Ferret studies

Similar to the hamster study, 12 ferrets (six donor ferrets and six transmission I ferrets) from the FLI in-house breeding were housed pairwise in strictly separated cages to prevent spillover contamination. Of these, six ferrets were inoculated with an equal 250 µl mixture of SARS-CoV-2 wt-S^{614G} and Alpha. The inoculum was back-titrated and the ratio of each variant was determined by RT-qPCR. The wt-S^{614G} vs Alpha mixture held a 1:1.2 ratio with $10^{5.875}$ $TCID_{50}$ distributed equally into each nostril of donor ferrets. Ferrets were separated for the first 24 hours following inoculation. Subsequently, the ferret pairs were co-housed again, allowing direct contact of donor to contact I ferrets. All ferrets were sampled via nasal washings with 750 µl PBS per nostril under a short-term inhalation anesthesia. Donor ferrets were sampled until euthanasia at 6 dpi, which was followed by the introduction of one additional naïve contact II ferret per cage (n=6), resulting in a 1:1 pairwise setup with contact I and II ferrets (Extended Data Fig. 2b). All ferrets, which were in the study group on the respective days, were sampled on the indicated days. Bodyweight, temperature, and physical condition of all animals were monitored daily throughout the experiment. URT and LRT organ samples, as well as blood samples of all ferrets were taken at respective euthanasia time points.

Full autopsy was performed on all animals under BSL3 conditions. The lung, trachea, and nasal conchae were collected and fixed in 10% neutral-buffered formalin for 21 days. The nasal atrium, decalcified nasal turbinates (cross-sections every 3-5 mm), trachea and all lung lobes were trimmed for paraffin embedding. Based on PCR results, tissue sections (3 µm) of all donors (day 6) and one recipient (# 8, day 20) were cut and stained with hematoxylin and eosin (H&E) for light microscopical examination. Immunohistochemistry (IHC) was performed using an anti-SARS nucleocapsid antibody (Novus Biologicals #NB100-56576, dilution 1:200) according to standardized avidin-biotin-peroxidase complex-method producing a red labelling and hematoxylin counterstain. For each immunohistochemistry staining, positive control slides and a negative control for the primary antibodies were included. Histopathology was performed on at least 5 consecutive tissue samples per animal, yielding comparable results in all cases. Lung tissue pathology was evaluated according to a detailed score sheet developed by Angele Breithaupt (DipECVP) (SI Table 2). Evaluation and interpretation was performed by board-certified veterinary pathologists (DiplECVP) (AB, IBV).

Mouse studies

Homozygous hACE2 knock-in mice (B6.Cg-*Ace2*$^{tm1(ACE2)Dwnt}$; henceforth hACE2-KI) and hemizygous transgenic mice (Tg(K18-hACE2)2Prlmn; henceforth hACE2-K18Tg) were described previously[3,18]. All mice were produced at the specific-pathogen-free facility of the Institute of Virology and Immunology (Mittelhäusern), where they were maintained in individually ventilated cages (blue line, Tecniplast), with 12-h/12-h light/dark cycle, 22 ± 1 °C ambient temperature and 50 ± 5% humidity, autoclaved food and acidified water. At least 7 days before infection, mice were placed in individually HEPA-filtered cages (IsoCage N, Tecniplast). Mice (10 to 12 weeks old) were anesthetized with isoflurane and infected intranasally with 20 µl per nostril with the virus inoculum described in the results section. One day after inoculation, infected hACE2-K18Tg mice were placed in the cage of another hACE2-K18Tg contact mouse. Mice were monitored daily for bodyweight loss and clinical signs. Oropharyngeal swabs were collected under brief isoflurane anesthesia using ultrafine sterile flock swabs (Hydraflock, Puritan, 25-3318-H). The tips of the swabs were placed in 0.5 ml of RA1 lysis buffer (Macherey-Nagel, ref. 740961) supplemented with 1% β-mercaptoethanol and vortexed. At 2 or 4 dpi, mice were euthanized, and organs were aseptically dissected. Systematic tissue sampling was performed as detailed previously[3].

Animal specimens work up, viral RNA detection, and quantification analyses

Organ samples from ferrets and hamsters were homogenized in a 1 ml mixture composed of equal volumes of Hank's balanced salts MEM and Earle's balanced salts MEM containing 2 mM L-glutamine, 850 mg l^{-1} NaHCO3, 120 mg l^{-1} sodium pyruvate, and 1% penicillin–streptomycin) at 300 Hz for 2 min using a Tissuelyser II (Qiagen) and centrifuged to clarify the supernatant. Organ samples from mice were either homogenized in 0.5 mL of RA1 lysis buffer supplemented with 1% β-mercaptoethanol using a Bullet Blender Tissue Homogenizer (Next-Advance Inc.) or in Tube M (Miltenyi Biotech, ref. 130-096-335) containing 1 mL of DMEM using a gentleMACS™ Tissue Dissociator (Miltenyi Biotech). Nucleic acid was extracted from 100 µl of the nasal washes or 200 µL mouse oropharyngeal swabs after a short centrifugation step or 100 µL of organ sample supernatant using the NucleoMag Vet kit (Macherey Nagel). Nasal washings, oropharyngeal swabs, and organ samples were tested by RT-qPCR analysis for the ratio of the

two different viruses used for inoculation, by applying two different assays, each of them specific for one variant: either the wt-S^{614G}, Alpha, or Beta variant (Extended Data Tables 2, 3). Viral RNA copies in swabs and organs in studies using a single variant inoculum in mice were determined using the E protein RT-qPCR exactly as described[3].

Four specific RT-qPCR assays for SARS-CoV-2 wt-S^{614G}, Alpha, and Beta were designed based on the specific genome deletions within the ORF1 and S gene (Extended Data Table 2). Here, virus specific primers were used to achieve a high analytical sensitivity (less than 10 genome copies/µl template) of the according PCR assays, also in samples with a high genome load of the non-matching virus.

The RT-qPCR reaction was prepared using the qScript XLT One-Step RT-qPCR ToughMix (QuantaBio, Beverly, MA, USA) (hamsters and ferrets) or the AgPath-ID™ One-Step RT-PCR (ThermoFisher Scientific) (hACE2-K18Tg and hACE2-KI mice) in a volume of 12.5 µl including 1 µl of the respective FAM mix and 2.5 µl of extracted RNA. The reaction was performed for 10 min at 50 °C for reverse transcription, 1 min at 95 °C for activation, and 42 cycles of 10 sec at 95 °C for denaturation, 10 sec at 60 °C for annealing and 20 sec at 68 °C for elongation. Fluorescence was measured during the annealing phase. RT-qPCRs were performed on a BioRad real-time CFX96 detection system (Bio-Rad, Hercules, USA) (hamsters and ferrets) or an Applied Biosystems™ 7500 Real-Time PCR System (ThermoFisher Scientific) (mice). Validation work was performed in comparison to established protocols[31,34].

Serological tests of hamsters and ferrets

Serum samples from the wt-S^{614G} and Alpha co-inoculated animals were tested by ELISA for sero-reactivity against the RBD domain[35] using a Tecan i-control 2014 1.11 plate reader and data was analyzed using Microsoft Excel 16.0. All samples were generated at the time point of euthanasia of the individual animal.

Statistical Analysis

Statistical analysis was performed using the GraphPad Prism version 8 or R (version 4.1)[36], using the packages tidyverse (v1.3.1)[37], ggpubr (v0.4.0)[38], rstatix (v.0.7.0)[39]. Unless noted otherwise, the results are expressed as means ± standard deviation (SD). Two-way ANOVA with Tukey Honest Significance Differences (HSD) post-hoc test was used to compare competition results at different time points post infection in vitro. One-way ANOVA with Tukey's multiple comparisons test was used to compare viral genome copies or titers at different time points post infection in individual virus mouse infection studies. Significance was defined as $p<0.05$.

Reporting summary

Further information on research design is available in the Nature Research Reporting Summary linked to this paper.

Data availability

Sequence data are available on the NCBI Sequence Read Archive (SRA) under the accession numbers PRJEB45736, and PRJNA784099, or in GenBank under the accession numbers MT108784, MZ433432, OL675863, OL689430, and OL689583 as shown in Extended Data Table 1. Source data are provided with this paper.

25. Hoffmann, M. et al. SARS-CoV-2 Cell Entry Depends on ACE2 and TMPRSS2 and Is Blocked by a Clinically Proven Protease Inhibitor. *Cell* **181**, 271-280 e278, https://doi.org/10.1016/j.cell.2020.02.052 (2020).
26. Thi Nhu Thao, T. et al. Rapid reconstruction of SARS-CoV-2 using a synthetic genomics platform. *Nature* **582**, 561-565, https://doi.org/10.1038/s41586-020-2294-9 (2020).
27. Wylezich, C., Papa, A., Beer, M. & Hoper, D. A Versatile Sample Processing Workflow for Metagenomic Pathogen Detection. *Sci Rep* **8**, 13108, https://doi.org/10.1038/s41598-018-31496-1 (2018).
28. Wylezich, C. et al. Next-generation diagnostics: virus capture facilitates a sensitive viral diagnosis for epizootic and zoonotic pathogens including SARS-CoV-2. *Microbiome* **9**, 51, https://doi.org/10.1186/s40168-020-00973-z (2021).
29. Essaidi-Laziosi, M. et al. Propagation of respiratory viruses in human airway epithelia reveals persistent virus-specific signatures. *J Allergy Clin Immunol* **141**, 2074-2084, https://doi.org/10.1016/j.jaci.2017.07.018 (2018).
30. V'Kovski, P. et al. Disparate temperature-dependent virus-host dynamics for SARS-CoV-2 and SARS-CoV in the human respiratory epithelium. *PLoS Biol* **19**, e3001158, https://doi.org/10.1371/journal.pbio.3001158 (2021).
31. Corman, V. M. et al. Detection of 2019 novel coronavirus (2019-nCoV) by real-time RT-PCR. *Euro Surveill* **25**, https://doi.org/10.2807/1560-7917.ES.2020.25.3.2000045 (2020).
32. Baggio, S. et al. SARS-CoV-2 viral load in the upper respiratory tract of children and adults with early acute COVID-19. *Clin Infect Dis*, https://doi.org/10.1093/cid/ciaa1157 (2020).
33. Jonsdottir, H. R. & Dijkman, R. Characterization of human coronaviruses on well-differentiated human airway epithelial cell cultures. *Methods Mol Biol* **1282**, 73-87, https://doi.org/10.1007/978-1-4939-2438-7_8 (2015).
34. https://www.who.int/docs/default-source/coronaviruse/real-time-rt-pcr-assays-for-the-detection-of-sars-cov-2-institut-pasteur-paris.pdf?sfvrsn=3662fcb6_2. *WHO*, <https://www.who.int/docs/default-source/coronaviruse/real-time-rt-pcr-assays-for-the-detection-of-sars-cov-2-institut-pasteur-paris.pdf?sfvrsn=3662fcb6_2> (2020).
35. Wernike, K. et al. Multi-species ELISA for the detection of antibodies against SARS-CoV-2 in animals. *Transbound Emerg Dis*, https://doi.org/10.1111/tbed.13926 (2020).
36. R: A language and environment for statistical computing (Vienna, Austria, 2021).
37. Wickham, H. et al. Welcome to the Tidyverse. *Journal of open source software* **4**, 1686 (2019).
38. ggpubr: 'ggplot2' Based Publication Ready Plots (2020).
39. rstatix: Pipe-Friendly Framework for Basic Statistical Tests (2021).

Acknowledgements We thank Frank Klipp, Doreen Fiedler, Christian Lipinski, and Steffen Kiepert (Friedrich-Loeffler-Institut); Katarzyna Sliz, and Daniel Brechbühl (Institute of Virology and Immunology) for animal care. We thank Mareen Lange, Christian Korthase, Patrick Zitzow, and Silvia Schuparis (Friedrich-Loeffler-Institut); Gianna Cadau, Paolo Valenti, Barbara Lemaitre (University Hospitals Geneva), Chantal Tougne, Paola Fontannaz, Pascale Sattonnet and Catia Alvarez (University of Geneva) for technical assistance. We thank M. Schmolke, B. Mazel-Sanchez, and F. Abdul (Faculty of Medicine, Geneva) for generously providing A549-hACE2 cells. This work was supported by grants from the Swiss National Science Foundation (SNSF), grants no. 31CA30_196062 (CB, RD), 31CA30_196644 (VT, IAE, RD), 310030_173085 (VT), 310030_179260 (RD), 196383 (IAE); the European Commission, Marie Skłodowska-Curie Innovative Training Network 'HONOURS', grant agreement no. 721367 (VT, RD); the European Union Project ReCoVer, grant no. GA101003589 (CDr); Core funds of the University of Bern (VT, RD); Core funds of the German Federal Ministry of Food and Agriculture (MB); the Deutsche Forschungsgemeinschaft (DFG), Project no. 453012513 (MB); the Horizon 2020 project "VEO", grant agreement no. 874735 (MB); COVID-19 special funds from the Swiss Federal Office of Public Health and the Swiss Federal Office of Food Safety and Veterinary Affairs (AS, VT); the Fondation Ancrage Bienfaisance du Groupe Pictet (IAE); the Fondation Privée des Hoˆpitaux Universitaires de Genève (IAE); the German Ministry of Research, VARIPath, grant no. 01KI2021 (VMC).

Author contributions Conceptualization: DH, MB, VT, CB. Data curation: LU, NJH, AT, NE, JS, CDe, BZ, RD. Funding acquisition: AS, IE, DEW, RD, VT, MB, CB. Investigation: LU, NJH, AT, NE, JS, CDe, BST, BH, MW, XF, MBek, MEL, MLS, DN, VMC, AK, AG, LL, JNK, BMC, AB, CW, IBV, MG, SO, BZ, KA, BM, CE, LT, MGA, RD, DH. Methodology: BH, AB, FL, JJ. Supervision: IE, CDr, RD, DH, VT, MB, CB. Visualization. LU, NJH, AT, JS, CDe, RD. Writing – original draft: LU, NJH, AT, RD, DH, MB, CB. Writing – review & editing: LU, NJH, AB, LT, RD, DH, VT, MB, CB

Competing interests The authors declare no competing interests.

Additional information

Supplementary information The online version contains supplementary material available at https://doi.org/10.1038/s41586-021-04342-0.

Correspondence and requests for materials should be addressed to Volker Thiel, Martin Beer or Charaf Benarafa.

Peer review information *Nature* thanks Stanley Perlman and the other, anonymous, reviewer(s) for their contribution to the peer review of this work. Peer reviewer reports are available.

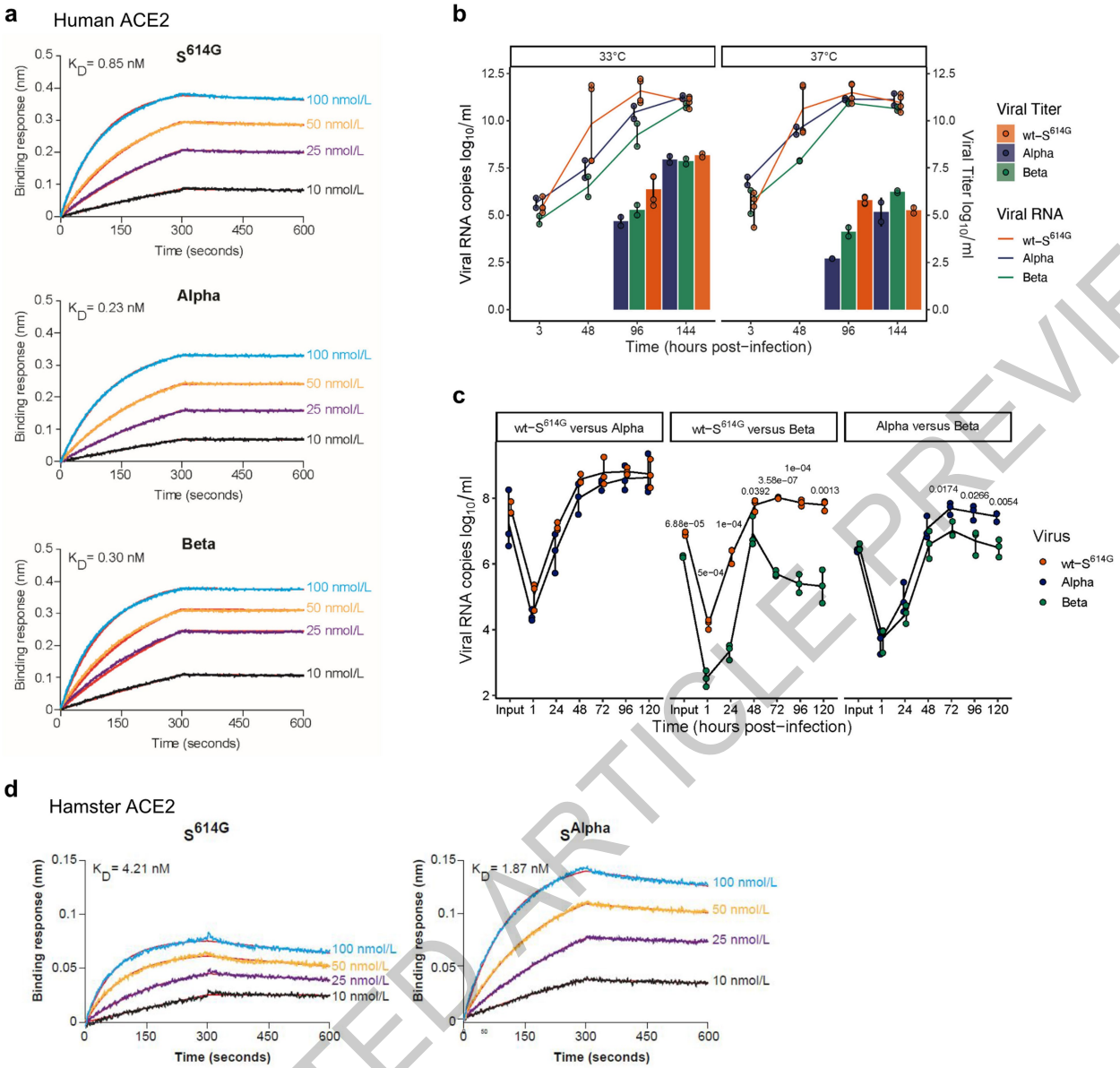

Extended Data Fig. 1 | ACE2 receptor binding and replication kinetics of SARS-CoV-2 VOC in vitro. (a) Affinity between spike (S^{614G}, S^{Alpha}, and S^{Beta}) protein trimers and hACE2 dimers determined by Bio-layer interferometry. (b) Viral replication kinetics of SARS-CoV-2 Alpha, Beta, and wt-S^{614G} (MOI 0.02) at 33 °C and 37 °C in primary human nasal airway epithelial cell (AEC) cultures. (c) Viral replication kinetics of pairwise competition assays in primary nasal AEC cultures at 33 °C (MOI 0.005). (b, c) Data are presented as individual points with mean (line) and standard deviation; (b) n=2 (Alpha and Beta), n=4 (wt-S^{614G}), (c) n=3 independent biological replicates. (c) P-values were determined by two-way ANOVA and Tukey Honest Significant Differences (HSD) post-hoc test. (d, e) Affinity between spike (S^{614G}, S^{Alpha}) protein trimers with hamster ACE2 (d) and ferret ACE2 (e) determined by Bio-layer interferometry. (a, d, e) ACE2 with IgG1 Fc tag were loaded on anti-human IgG Fc biosensors and binding kinetics were conducted using indicated concentrations of spike trimers. Data is representative of 3 independent experiments.

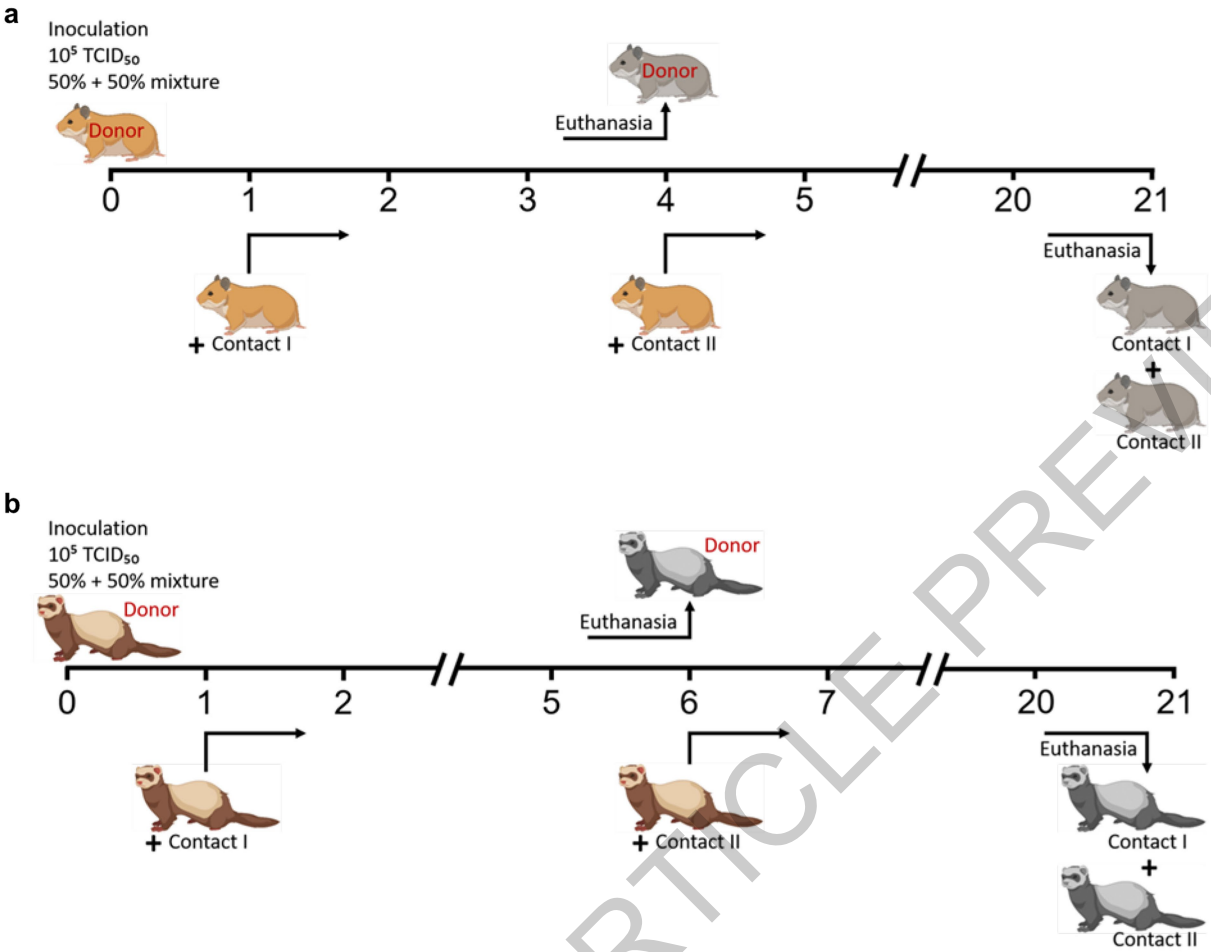

Extended Data Fig. 2 | Experimental workflow of competitive transmission experiments in Syrian hamsters and ferrets. (a) Timeline of the hamster experiments. Six intranasally inoculated donor hamsters each were co-housed with one naïve contact hamster (1 dpi), building six respective donor-contact I pairs. At 4 dpi, the donor hamsters were euthanized and the initial contact hamsters I were co-housed with one additional hamster (Contact II). (b) Timeline of the ferret experiment. The scheme was generated with BioRender (https://biorender.com/).

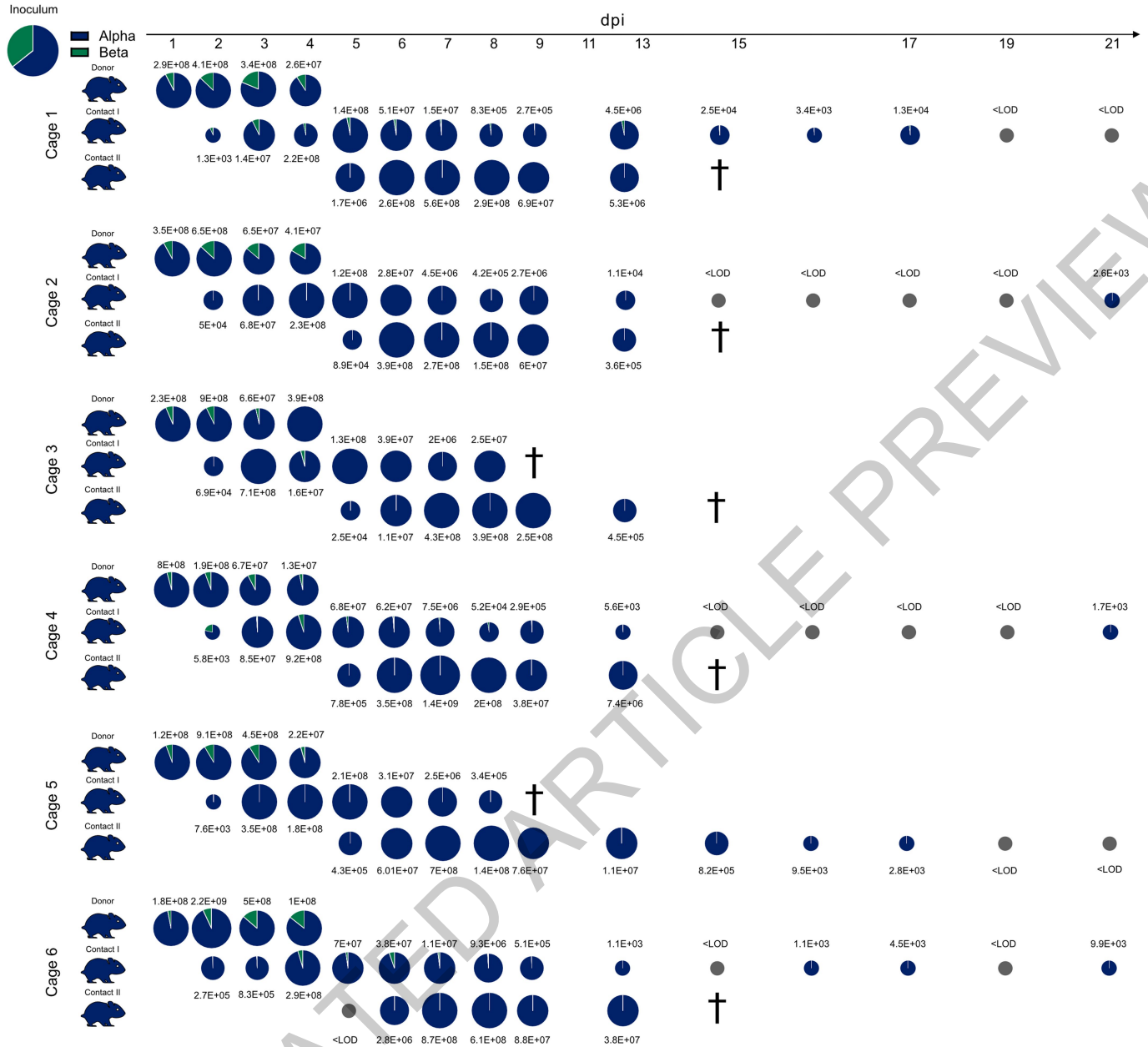

Extended Data Fig. 3 | Competitive transmission between Alpha and Beta in Syrian hamsters. Six donor hamsters were each inoculated with $10^{5.06}$ $TCID_{50}$ determined by back titration and composed of a mixture of Alpha (dark blue) and Beta (green) at 1.8:1 ratio determined by RT-qPCR. Donor hamsters, contact I and II hamsters were co-housed sequentially as shown in Extended Data Figure 2a. Nasal washings were performed daily from 1-9 dpi and afterwards every two days until 21 dpi. Pie chart colors illustrate the ratio of variants detected in nasal washings at the indicated dpi. Pie chart sizes are proportional to the total viral genome copies reported above or below respective pies. Grey pies indicate values below the LOD (<103 viral genome copies per sample). Hamster silhouettes are colored according to the dominant variant (>66%) detected in the latest sample of each animal. † indicate that the corresponding animal reached the humane endpoint.

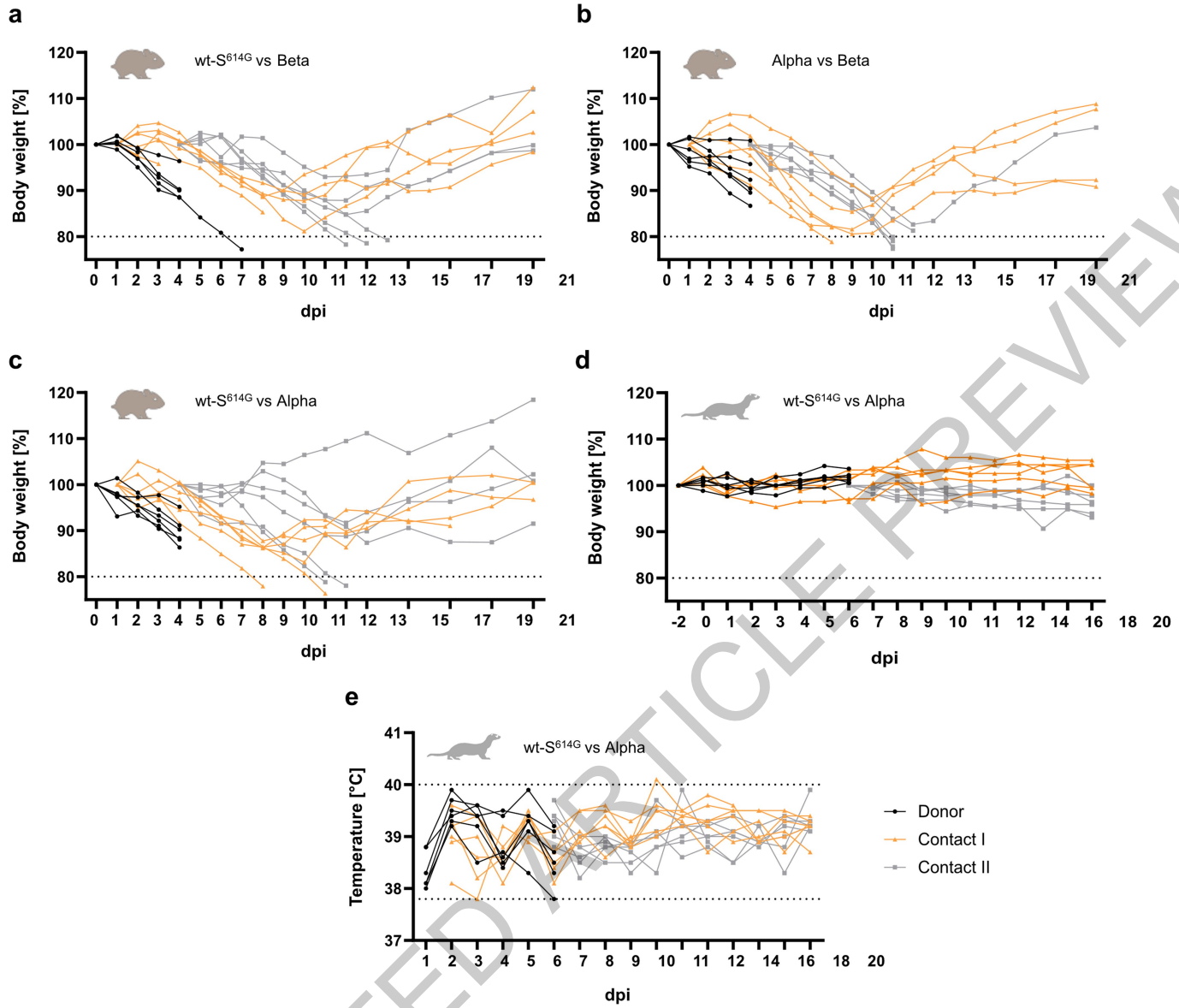

Extended Data Fig. 4 | Clinical features of hamsters and ferrets. (a-c) Syrian hamsters were inoculated with comparable genome equivalent mixture of either wt-S^{614G} and Beta (a), Alpha and Beta (b), or wt-S^{614G} and Alpha (c). In hamsters, body weight was monitored daily until 13 dpi, afterwards every two days until 21 dpi and plotted relative to bodyweight of day 0. The dotted line indicates the humane endpoint criterion of 20% body weight loss from initial bodyweight at which hamsters were promptly euthanized for animal welfare reasons. (d, e) Ferrets were inoculated intranasally with an equal mixture of wt-S^{614G} and Alpha. Body weight (d) and temperature (e) were monitored daily in ferrets until 12 dpi, and afterwards every 2 days. Grey dotted lines in e indicate the physiologic range for body temperature in ferrets.

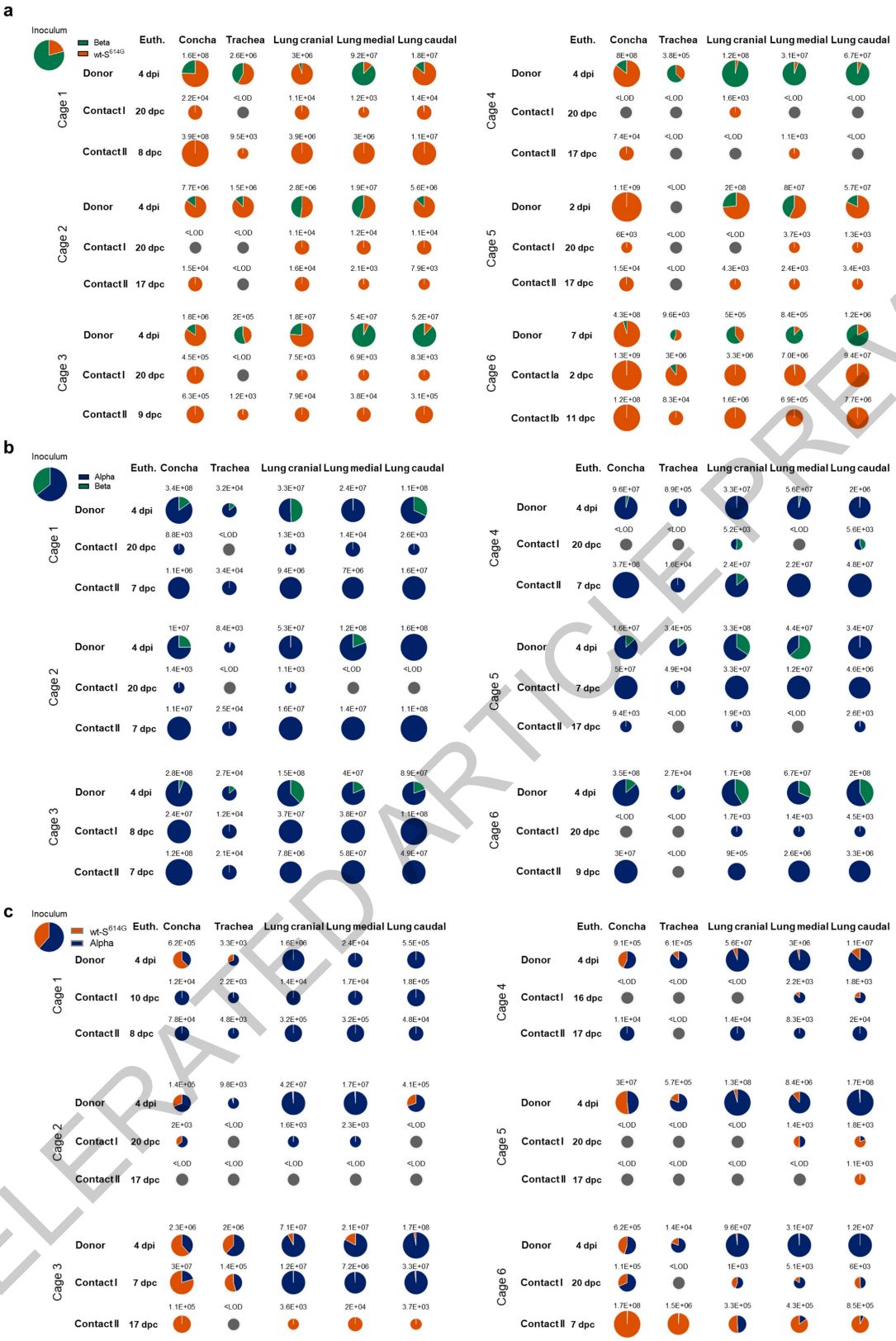

Extended Data Fig. 5 | Viral genome load in upper (URT) and lower (LRT) respiratory tract tissues of Syrian hamsters in the competitive transmission experiment between SARS-CoV-2 VOCs. (a-c) Syrian hamsters were inoculated with comparable genome equivalent mixture of either wt-S^{614G} and Beta (a), Alpha and Beta (b), or wt-S^{614G} and Alpha (c). Absolute quantification was performed by RT–qPCR analysis of tissue homogenates of donor, contact I and contact II hamsters in relation to a set of defined standards. Tissue samples were collected at euthanasia (Euth.). Pie chart colors illustrate the ratio of variants detected in each sample at the indicated dpi or days post contact (dpc). Pie chart sizes are proportional to the total viral genome copies reported below. Grey pies indicate values below the LOD (<10^3 viral genome copies per sample).

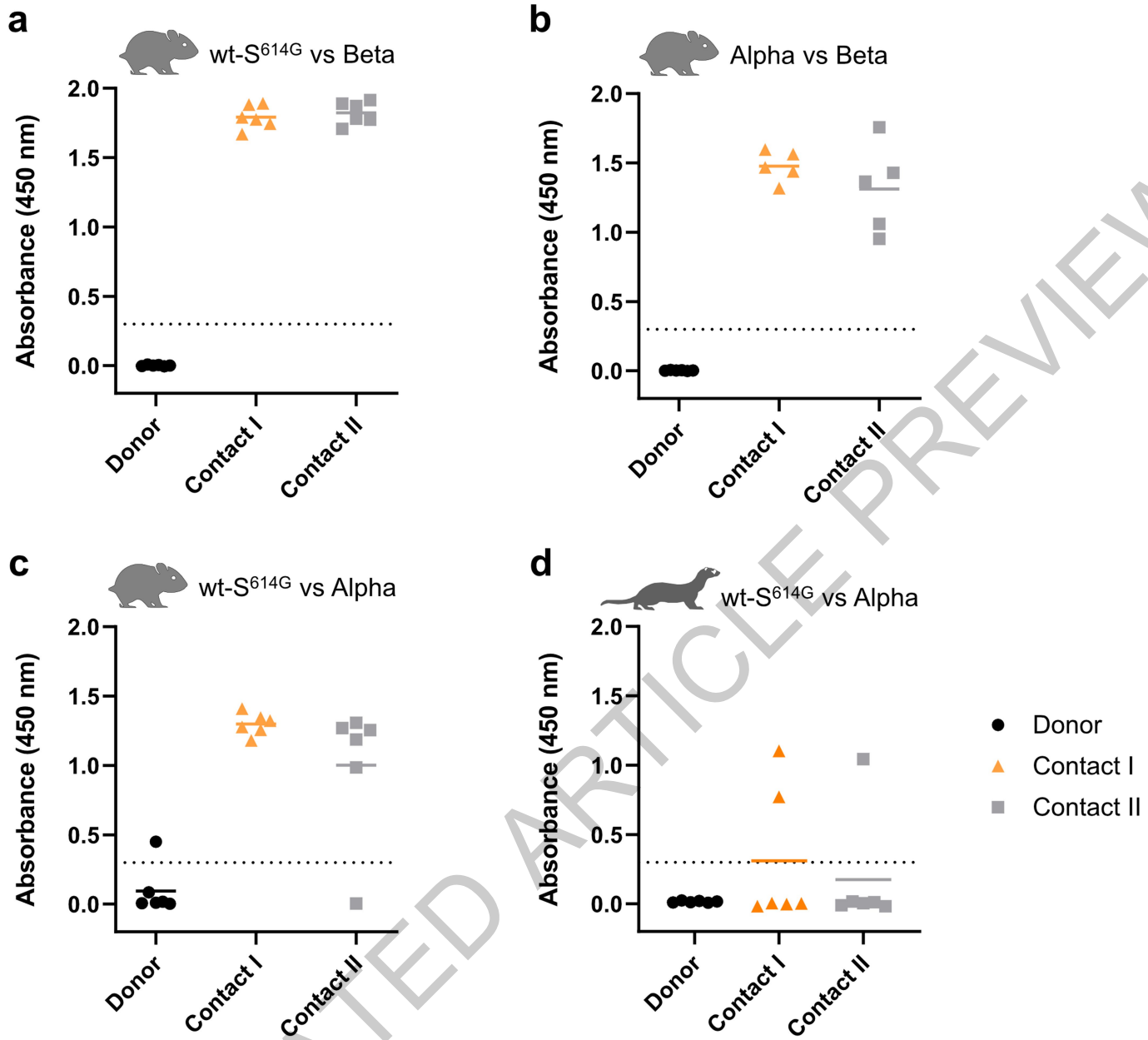

Extended Data Fig. 6 | Indirect ELISA against the RBD of SARS-CoV-2. Sera of donor hamsters (a, b, c) and ferrets (d) inoculated with the indicated SARS-CoV-2 VOC mixtures and sera of contact I and II animals were collected at their respective experimental endpoints . All sera were tested for specific reactivity against the SARS-CoV-2 RBD-SD1 domain (wt-S amino acids 319-519).

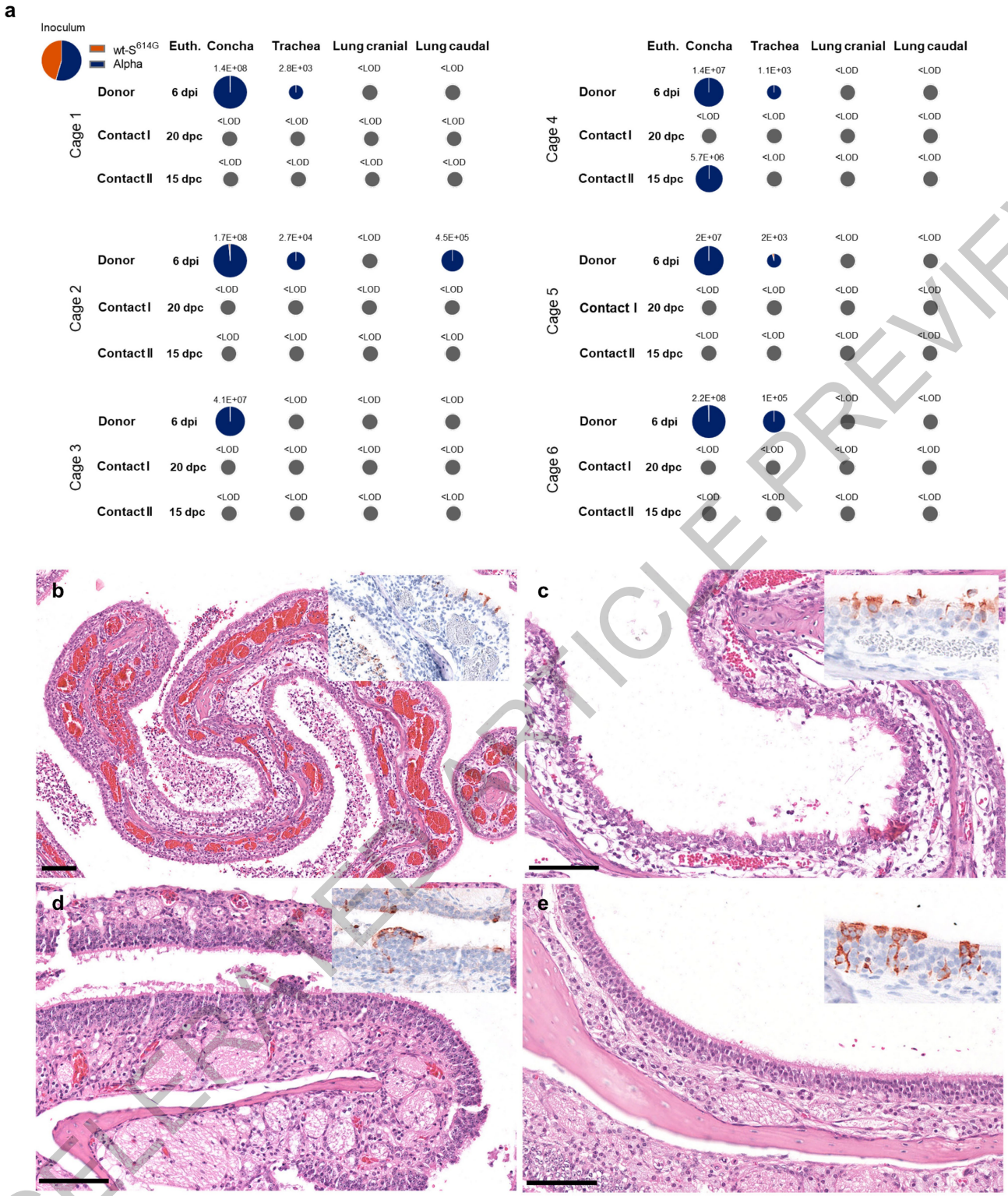

Extended Data Fig. 7 | Viral genome load in upper (URT) and lower (LRT) respiratory tract tissue of ferrets in the competitive transmission experiment between SARS-CoV-2 Alpha and wt-S^{614G}. (a) Absolute quantification was performed by RT–qPCR analysis of tissue homogenates of donor, contact I and contact II ferrets in relation to a set of defined standards. Tissue samples were collected at euthanasia (Euth.). Pie chart colors illustrate the ratio of variants detected in each sample at the indicated dpi or dpc. Pie chart sizes are proportional to the total viral genome copies reported below. Grey pies indicate values below the LOD (<10^3 viral genome copies per sample). (b-e) Representative micrographs of hematoxylin and eosin staining of 3 µm sections of nasal conchae of donor ferrets (n=6) 6 dpi with wt-S^{614G} and Alpha. Micrographs are representative of 5 consecutive tissue samples of each animal. Insets show immunohistochemistry staining of SARS-CoV-2 with anti-SARS nucleocapsid antibody with hematoxylin counterstain. The respiratory (b, c) and olfactory (d, e) nasal mucosa exhibited rhinitis with varying severity. Lesion-associated antigen was found in ciliated cells of the respiratory epithelium (b, c) and in sustentacular cells of the olfactory epithelium (d, e) in all donor animals (n=6) at 6 dpi. Scale bars are 100 µm.

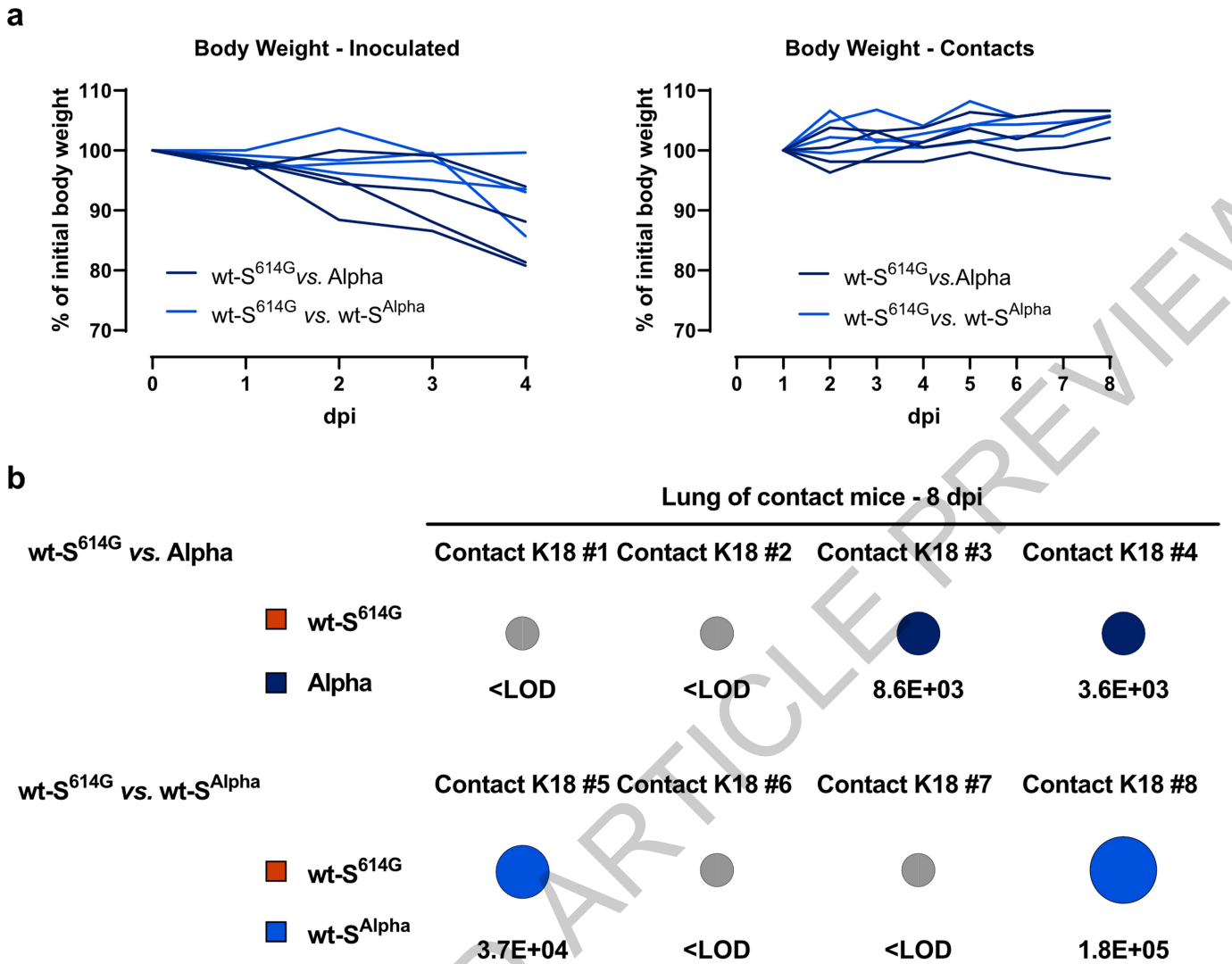

Extended Data Fig. 8 | Bodyweight and transmission in hACE2-K18Tg mice. hACE2-K18Tg mice inoculated with a mixture of wt-S^{614G} and Alpha, or wt-S^{614G} and wt-S^{Alpha}. (a) Relative body weight of individual donor mice (n=4mice/group; left panel), and contact mice (n=4mice/group; right panel). (b) Pie chart colors illustrate the ratio of wt-S^{614G} (orange) with Alpha (dark blue), or with wt-S^{Alpha} (light blue) in corresponding experiments in lung homogenates of contact mice at 7 dpc (i.e., 8 dpi of donor mice). Pie chart sizes are proportional to the total viral genome copies reported below. Grey pies indicate values below the LOD (<10^3 viral genome copies per sample).

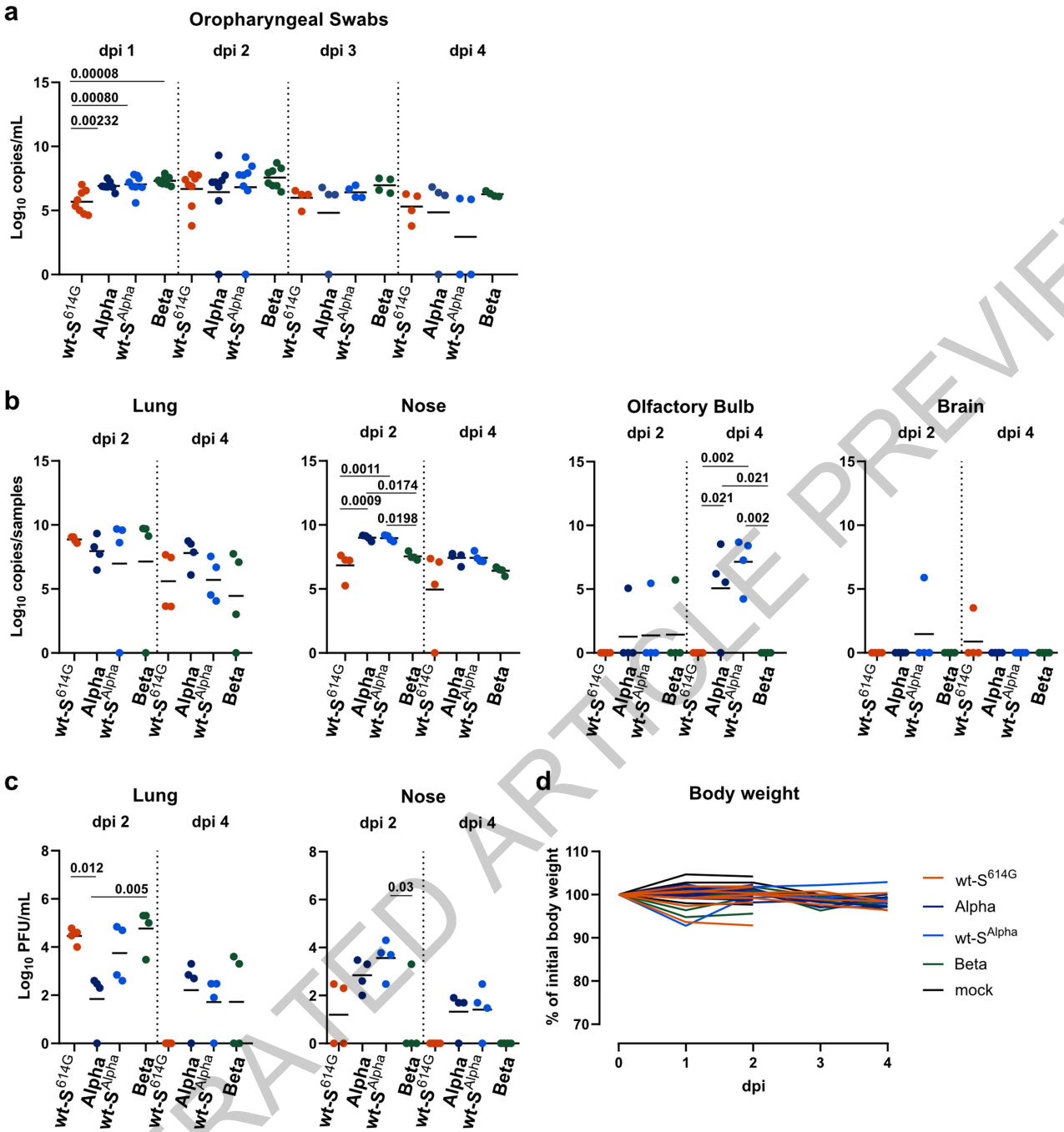

Extended Data Fig. 9 | Replication of VOC in hACE2-KI mice. (a-d) Groups hACE2-KI male mice were inoculated intranasally with 10^4 PFUs of SARS-CoV-2 wt-S^{614G}, Alpha, wt-S^{Alpha} and Beta (n=8 mice/group). Genome copy numbers in daily oropharyngeal swabs (a) and in tissues (b), and virus titers (c) in tissues were determined at indicated dpi. Data were log10 transformed and presented as individual values and mean. * $p<0.05$, ** $p<0.01$ by one-way ANOVA with Tukey's multiple comparisons test comparing the four groups. (d) Relative body weight of individual hACE2-KI mice overtime relative to weight at infection (n = 8 mice/group until 2 dpi, and n= 4 mice/group from 3 dpi).

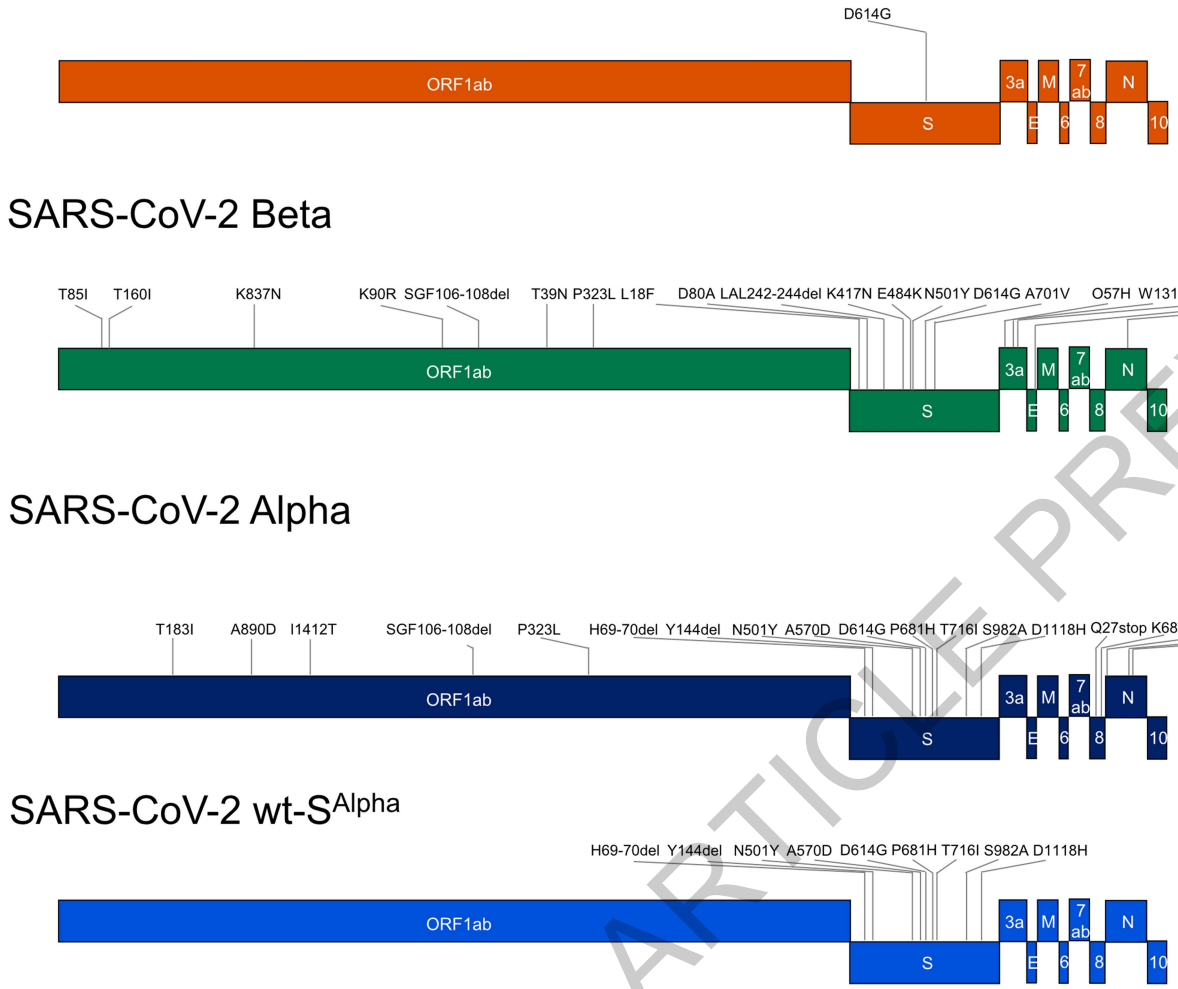

Extended Data Fig. 10 | Genome sequences of used SARS-CoV-2 variants. Colors of the variants represent respective viruses in the different experiments. Grey lines indicate positions of known mutations of each virus strain.

Extended Data Table 1 | Sequence mutations in S in SARS-CoV-2 recombinant strains

SARS-CoV-2 viruses	Mutations in S	Use	Accession ID (BioProject / GenBank / GISAID)
Isolates:			
wt-S^{614G} (B.1.610)	D614G	Kinetics in vitro	OL675863, EPI_ISL_414019
Alpha	H69/V70del, Y144del, N501Y, A570D, D614G, P681H, T716I, S982A, D1118H	Kinetics in vitro	OL689430, EPI_ISL_2131446
Beta	L18F, D80A, D215G, L242/A243/L244del, K417N, E484K, N501Y, D614G, A701V,	Kinetics in vitro	OL689583, EPI_ISL_981782
Alpha (L4549)	H69/V70del, Y144del, N501Y, A570D, D614G, P681H, T716I, S982A, D1118H	Competition wt-S^{614G} vs Alpha; in vitro, hamster, ferret, and mice Individual virus infection, mice	PRJEB45736, SARS-CoV-2 B.1.1.7 NW-RKI-I-0026/2020 passage 3 L4549, EPI_ISL_803957
Beta (L4550) (Ref. 21)	L18F, D80A, D215G, L242/L243/A244del K417N, E484K, N501Y, D614G, A701V	Competition wt-S^{614G} vs Beta; hamster, mice Competition Alpha vs Beta; hamster	MZ433432, L4550, EPI_ISL_751799
Recombinant clones:			
wt-S^{614G} (Ref. 3)	D614G	Competition wt-S^{614G} vs Beta; in vitro, hamster, mice Competition wt-S^{614G} vs Alpha; in vitro, mice Competition wt-S^{614G} vs wt-S^{Alpha}; mice Single virus infection, mice	MT108784
wt-S^{614G} (*) (L4595)	D614G, R685S	Competition wt-S^{614G} vs Alpha; hamster and ferret	PRJEB45736, wt-S614G ID#49 vial 2, L4595
wt-S^{Alpha}	H69/V70del, Y144del, N501Y, A570D, D614G, P681H, T716I, S982A, D1118H	Competition wt-S^{614G} vs wt-S^{Alpha}; mice Single virus infection, mice	PRJNA784099

(*) SARS-CoV-2 wt-S^{614G} used for the competitive experiments between wt-S^{614G} vs. Alpha in hamsters and ferrets had an exchange in 54% of the analyzed contigs from C to A in position 23615, located in the S gene.

Extended Data Table 2 | Sequences of primer and probes for RT-qPCR assays

Oligo name	Sequence (5′- 3′)	Conc.	Position
SARS-CoV-2 wt-S^{614G} -ORF1 assay			
wt-S^{614G} -ORF1-1.2F	TGG TTG ATA CTA GTT TGT CTG GT	10 µM	11271-11293 *
wt-S^{614G} -ORF1-1.3R	GCA CCA TCA TCA TAC ACA GTT C	10 µM	11379-11358 *
wt-S^{614G} -ORF1-1FAM	FAM-TGC ATC AGC TGT AGT GTT ACT AAT CC-BHQ1	5 µM	11320-11345 *
SARS-CoV-2 wt-S^{614G} -S assay			
wt-S^{614G} -S-1.2F	TAC TTG GTT CCA TGC TAT ACA TGT	10 µM	21748-21771 *
wt-S^{614G} -S-1.5R	CCA ACT TTT GTT GTT TTT GTG GTA ATA	10 µM	22018-21992 *
wt-S^{614G} -S-1FAM	FAM-ACC CTG TCC TAC CAT TTA ATG ATG-BHQ1	5 µM	21804-21827 *
SARS-CoV-2 Alpha -ORF1 assay			
B117-ORF1-2.1F	GAT ATG GTT GAT ACT AGT TTG AAG	10 µM	11265-11288 **
wt-S^{614G} -ORF1-1.3R	See above		
wt-S^{614G} -ORF1-1FAM	See above		
SARS-CoV-2 Alpha -S assay			
B117-S-1.2F	TTA CTT GGT TCC ATG CTA TMT C	10 µM	21736-21757 **
B117-S-1.3R	AAC TTT TGT TGT TTT TGT GGT AAA C	10 µM	21996-21972 **
wt-S^{614G} -S-1FAM	See above		

* Position based on NC_045512; ** Position based on MW963651. Conc, concentration.

Extended Data Table 3 | Attribution of RT-qPCR assays used for the individual competitive transmission experiments

Assay	For detection of
wt-S^{614G} vs Alpha (hamsters, ferrets)	
SARS-CoV-2 wt-S^{614G} -ORF1 assay	SARS-CoV-2 wt-S^{614G}
SARS-CoV-2 Alpha -ORF1 assay	SARS-CoV-2 Alpha
wt-S^{614G} vs Alpha (human AEC cultures, mice)	
SARS-CoV-2 wt-S^{614G} -S assay	SARS-CoV-2 wt-S^{614G}
SARS-CoV-2 Alpha -S assay	SARS-CoV-2 Alpha
SARS-CoV-2 Alpha -S assay	SARS-CoV-2 wt-S^{Alpha}
wt-S^{614G} vs Beta (human AEC cultures, hamsters and mice)	
SARS-CoV-2 wt-S^{614G} -ORF1 assay	SARS-CoV-2 wt-S^{614G}
SARS-CoV-2 Alpha -ORF1 assay	SARS-CoV-2 Beta
Alpha vs Beta (human AEC cultures, hamsters)	
SARS-CoV-2 Alpha -S assay	SARS-CoV-2 Alpha
SARS-CoV-2 wt-S^{614G} -S assay	SARS-CoV-2 Beta

nature portfolio

Corresponding author(s): Charaf Benarafa
Martin Beer
Volker Thiel

Last updated by author(s): Nov 26, 2021

Reporting Summary

Nature Portfolio wishes to improve the reproducibility of the work that we publish. This form provides structure for consistency and transparency in reporting. For further information on Nature Portfolio policies, see our Editorial Policies and the Editorial Policy Checklist.

Statistics

For all statistical analyses, confirm that the following items are present in the figure legend, table legend, main text, or Methods section.

n/a	Confirmed	
☐	☒	The exact sample size (*n*) for each experimental group/condition, given as a discrete number and unit of measurement
☐	☒	A statement on whether measurements were taken from distinct samples or whether the same sample was measured repeatedly
☐	☒	The statistical test(s) used AND whether they are one- or two-sided *Only common tests should be described solely by name; describe more complex techniques in the Methods section.*
☐	☒	A description of all covariates tested
☐	☒	A description of any assumptions or corrections, such as tests of normality and adjustment for multiple comparisons
☐	☒	A full description of the statistical parameters including central tendency (e.g. means) or other basic estimates (e.g. regression coefficient) AND variation (e.g. standard deviation) or associated estimates of uncertainty (e.g. confidence intervals)
☐	☒	For null hypothesis testing, the test statistic (e.g. *F*, *t*, *r*) with confidence intervals, effect sizes, degrees of freedom and *P* value noted *Give P values as exact values whenever suitable.*
☒	☐	For Bayesian analysis, information on the choice of priors and Markov chain Monte Carlo settings
☒	☐	For hierarchical and complex designs, identification of the appropriate level for tests and full reporting of outcomes
☒	☐	Estimates of effect sizes (e.g. Cohen's *d*, Pearson's *r*), indicating how they were calculated

Our web collection on statistics for biologists contains articles on many of the points above.

Software and code

Policy information about availability of computer code

Data collection	ELISA: Tecan i-control 2014 1.11 qRT-PCR: QuantStudio™ Real-Time PCR Software (v1.7.1), or 7500 Fast System SDS Software Version 1.4 Viral titers: manual counting, registered in Microsoft Excel 2016 (16.0.5239.1001) BLI: Octet RED96e instrument with ForteBio Data Acquisition Software (Version: 12.0.1.8)
Data analysis	relative variant quantification: Bio-Rad CFX Maestro 1.1 Version 4.1.2433.1219 sequence analysis: Geneious Prime ® 2019.2.3 figures: GraphPad Prism 8.4.2 (679) for Windows, Microsoft PowerPoint 2016 (16.0.4266.1001), Adobe Photoshop CS5 64 bit NGS: Genome Sequencer Software Suite (version 2.6; Roche, https://roche.com), variant analysis tool integrated in Geneious Prime (2019.2.3) digital PCR: QuantaSoft Analysis Pro software (version 1.0.596) ELISA: Microsoft Excel 2016 (16.0.5188.1000) Statistical analysis: GraphPad Prism version 8 or R (version 4.1), using the packages tidyverse (v1.3.1), ggpubr (v0.4.0), rstatix (v.0.7.0). BLI: ForteBio Data Analysis Software (Version 12.0.1.2)

For manuscripts utilizing custom algorithms or software that are central to the research but not yet described in published literature, software must be made available to editors and reviewers. We strongly encourage code deposition in a community repository (e.g. GitHub). See the Nature Portfolio guidelines for submitting code & software for further information.

Data

Policy information about availability of data

All manuscripts must include a data availability statement. This statement should provide the following information, where applicable:

- Accession codes, unique identifiers, or web links for publicly available datasets
- A description of any restrictions on data availability
- For clinical datasets or third party data, please ensure that the statement adheres to our policy

Sequence data are available on the NCBI Sequence Read Archive (SRA) under the accession numbers PRJEB45736, and PRJNA784099, or in GenBank under the accession numbers MT108784, MZ433432, OL675863, OL689430, and OL689583 as shown in Extended Data Table 1. Source data are provided with this paper.

Field-specific reporting

Please select the one below that is the best fit for your research. If you are not sure, read the appropriate sections before making your selection.

☒ Life sciences ☐ Behavioural & social sciences ☐ Ecological, evolutionary & environmental sciences

For a reference copy of the document with all sections, see nature.com/documents/nr-reporting-summary-flat.pdf

Life sciences study design

All studies must disclose on these points even when the disclosure is negative.

Sample size	No sample size calculations were performed. Number of animals used in experiments were based on our previous comparative studies of fitness of SARS-CoV-2 variants.
Data exclusions	No data were excluded from analysis.
Replication	Binding Assays (BLI): data are representative of 3 independent experiments. Airway epithelial cell (AEC) cultures in vitro: All attempts at replication were successful; experiments were performed independently on different biological donors according to best practices and as described in the Methods. In vivo: Competition experiments between two VOCs were performed on groups of 6 infected animals and replicated in 4 animal models. Competition between wt-S614G and Alpha was replicated in males and females. All attempts at replication were successful. Single VOC infections were performed in groups of 8 mice for each variant.
Randomization	No randomization was required for all in vitro and in vivo competition experiments because the viral and host response parameters were measured within each cell culture insert or each animal. For single infection with VOCs, hACE2-KI were randomly assigned to the respective study groups.
Blinding	Investigators were blinded during analysis of viral plaque and qRT-PCR assays of in vitro and in vivo experiments. Blinding was also not relevant for in vivo competition experiments as both arms of the comparison were in single animals.

Reporting for specific materials, systems and methods

We require information from authors about some types of materials, experimental systems and methods used in many studies. Here, indicate whether each material, system or method listed is relevant to your study. If you are not sure if a list item applies to your research, read the appropriate section before selecting a response.

Materials & experimental systems

n/a	Involved in the study
☐	☒ Antibodies
☐	☒ Eukaryotic cell lines
☒	☐ Palaeontology and archaeology
☐	☒ Animals and other organisms
☒	☐ Human research participants
☒	☐ Clinical data
☒	☐ Dual use research of concern

Methods

n/a	Involved in the study
☒	☐ ChIP-seq
☒	☐ Flow cytometry
☒	☐ MRI-based neuroimaging

Antibodies

Antibodies used	anti-SARS nucleocapsid antibody (Novus Biologicals #NB100-56576)

Validation	relevant validation information can be accessed at https://www.novusbio.com/products/sars-nucleocapsid-protein-antibody_nb100-56576#reviews-publications

Eukaryotic cell lines

Policy information about cell lines

Cell line source(s)	Vero E6 cells (FLI): Collection of Cell Lines in Veterinary Medicine CCLV RIE 0929 Vero E6 cells (IVI, IFIK): cells were kindly provided by Doreen Muth, Marcel Müller, and Christian Drosten, Charité, Berlin, Germany (ATCC CRL-1586) Vero-TMPRSS2 cells were kindly provided by Stefan Pöhlmann, German Primate Center - Leibniz Institute for Primate Research, Göttingen, Germany) Primary human nasal cells were commercially procured from Epithelix, in Geneva, Switzerland. Expi293F cells: ThermoFisher Scientific, USA. A549-hACE2 cells were derived from ATCC CCL-185 and kindly provided by M. Schmolke, B. Mazel-Sanchez, and F. Abdul, Faculty of Medicine, Geneva
Authentication	in-house authentication for cell lines was not performed
Mycoplasma contamination	Cell lines were tested negative for mycoplasma contamination.
Commonly misidentified lines (See ICLAC register)	None

Animals and other organisms

Policy information about studies involving animals; ARRIVE guidelines recommended for reporting animal research

Laboratory animals	Mustela putorius furo, ferrets, neutered male and female, 8 - 23 months Mesocricetus auratus, Syrian hamster, male, 7-12 weeks Mus musculus, mice B6.Cg-Tg(K18-ACE2)2Prlmn/J, male and female, 10-12 weeks Mus musculus, mice B6.Cg-Ace2<tm1(ACE2)Dwnt>, male and female, 10-12 weeks
Wild animals	No wild animals were used
Field-collected samples	Field samples were not collected
Ethics oversight	Ferrets/hamsters: State Office of Agriculture ethics committee, Food Safety, and Fishery in Mecklenburg–Western Pomerania, Germany, registration number LVL MV TSD/7221.3-1-004/21 Mice: Commission for Animal Experimentation, Cantonal Veterinary Office of Bern, Switzerland, license BE-43/20

Note that full information on the approval of the study protocol must also be provided in the manuscript.